mathematics

MDPI

Article

Dynamics of Information–Epidemic Coupled Spreading in Age-Heterogeneous Multilayer Networks

Xiujuan Ma [1,2,*], Zhijia Liu [1,2], Fuxiang Ma [1,2], Xin Yang [1,2] and Lianzheng Wu [1,2]

[1] The College of Computer Science, Qinghai Normal University, Xining 810016, China
[2] The State Key Laboratory of Tibetan Intelligent Information Processing and Application, Xining 810008, China
* Correspondence: qhnumaxiujuan@163.com

Abstract

To investigate the interaction between protective information diffusion and disease transmission, this study proposes an information–epidemic coupled spreading model on an age-heterogeneous multilayer network. The population is divided into three age groups: youth, middle-aged individuals, and older adults. Disease transmission and protective information diffusion are represented in the physical disease layer and the virtual information layer, respectively. A UA-SIR framework is adopted to describe the coupled evolution of nodes' information awareness states and epidemic states. The model further incorporates age-specific spreading parameters, the effects of awareness on infection risk and recovery processes, and the feedback effect of infection status on information diffusion. Node-level state transition equations are established, and the epidemic threshold is analyzed using an age-aggregated next-generation matrix. Simulation results show that age-dependent information diffusion, infection-induced feedback, the initial location of information seeds, and network topology all affect the epidemic spreading process. Empirical analyses based on four real infectious disease datasets further indicate that introducing information diffusion can reduce the infection peak, flatten the epidemic curve, and delay the peak time in some scenarios. These findings provide theoretical insights into age-stratified information intervention strategies in heterogeneous populations.

Keywords: information–epidemic coupled spreading; age heterogeneity; multilayer networks; UA-SIR model; epidemic threshold

MSC: 92D30; 60J20

Check for updates

Academic Editor: Roman Ivanovich Parovik

Received: 24 June 2026
Revised: 22 July 2026
Accepted: 28 July 2026
Published: 2 August 2026

Copyright: © 2026 by the authors. Licensee MDPI, Basel, Switzerland. This article is an open access article distributed under the terms and conditions of the Creative Commons Attribution (CC BY) license.

1. Introduction

The spread of infectious diseases is influenced not only by pathogen transmissibility, individual immunity, and contact network structure, but also by public risk perception, access to protective information, and behavioral responses. The classical susceptible–infected–recovered (SIR) model provides a fundamental framework for epidemic modeling. Its core idea is to divide the population into susceptible, infected, and recovered individuals and to describe epidemic evolution through state transitions [1]. However, classical compartmental models are usually based on the homogeneous mixing assumption, which makes it difficult to capture heterogeneity in individual contact patterns, information acquisition, and protective behaviors in real societies. With the development of complex network theory, epidemic processes have increasingly been embedded in social contact

networks, revealing the effects of degree distribution, clustering structure, hub nodes, and community structure on epidemic thresholds, infection scale, and spreading speed [2–4].

Real-world spreading processes are inherently multilayered. On the one hand, diseases mainly spread through physical contact networks, such as households, schools, workplaces, and communities. On the other hand, protective information diffuses through virtual or semi-virtual channels, including social media, instant messaging, news platforms, and offline communication. Multilayer network theory provides an effective framework for describing different types of relationships and their interactions [5,6]. In studies of coupled information–epidemic spreading, many existing information–epidemic models assume that the information layer and the disease layer may have different topological structures, and the same individual may have different neighbors in different layers. Information diffusion can change individual protective behaviors, thereby reducing infection probability or improving compliance with medical treatment; conversely, an epidemic outbreak can increase public attention to preventive information and further promote information diffusion.

Previous studies have investigated the influence of awareness on epidemic spreading from different perspectives. Funk et al. [7] first incorporated the spread of awareness into epidemic models and showed that individuals may acquire risk information through observation and communication, even without centralized information release, and subsequently change their behaviors. Granell et al. [8,9] proposed coupled awareness–epidemic spreading models on multiplex networks, revealing the dynamic interplay between information diffusion and epidemic transmission and showing that awareness diffusion can alter epidemic outbreak thresholds. Subsequent studies further examined the effects of information forgetting, mass media, local risk perception, self-initiated protective behavior, different time scales, and network topology on coupled spreading processes [10–14]. In recent years, related research has been extended to more complex scenarios, such as selective mass media, awareness heterogeneity, temporal multilayer networks, information reception costs, and activity-driven individual behaviors [15–20]. These studies indicate that information diffusion is not merely an external factor in epidemic spreading, but rather an important dynamical mechanism that can coevolve with disease transmission and reshape both spreading intensity and spreading tempo. Recently, Gao et al. [21] investigated epidemic propagation dynamics on higher-order multilayer networks and demonstrated that higher-order interactions can significantly influence epidemic spreading patterns and epidemic thresholds. Their work provides an important extension of epidemic dynamics from traditional pairwise interactions to higher-order network structures. However, the study mainly focuses on the influence of higher-order interactions on disease propagation and does not explicitly consider the co-evolution between protective information diffusion and epidemic transmission, nor does it incorporate behavioral heterogeneity among different age groups.

Although existing models have provided important insights into coupled information–epidemic spreading, several aspects still require further investigation. First, many studies are based on general two-layer networks or homogeneous individual assumptions, with insufficient attention paid to age structure, household relationships, and cross-age contact heterogeneity. In real public health events, different age groups exhibit significant differences in social contact range, information channels, protective awareness, infection risk, and recovery capacity. Social contact surveys and age-specific contact matrix studies have shown that contact frequency and contact partners are strongly age-dependent, and that households, schools, and workplaces play important roles in infectious disease transmission [22,23]. Second, although some models introduce an information layer, they mainly focus on average infection size, epidemic thresholds, or overall information coverage, while the functional roles of different age groups in information seeding, cross-layer diffusion,

and prevention strategies remain insufficiently discussed. Third, many existing studies are mainly based on theoretical simulations, and comparative analyses using multiple types of real infectious disease data remain relatively limited.

To address these issues, this study constructs a UA-SIR information–epidemic coupled spreading model on an age-heterogeneous multilayer network. The population is divided into three age groups: youth, middle-aged individuals, and older adults. The disease layer is used to describe age-stratified physical contact relationships, while the virtual information layer is used to describe the diffusion of protective information. One-to-one interlayer node mapping is introduced to dynamically regulate disease-related parameters according to individuals' information states.

The main contributions of this study are as follows. First, an "information virtual layer–age-heterogeneous disease layer" multilayer modeling framework is constructed to distinguish information diffusion carriers from disease transmission carriers. Second, age-specific information-spreading rates, information forgetting rates, disease transmission rates, and recovery rates are incorporated into the UA-SIR coupled framework to characterize behavioral and spreading differences among age groups. Third, node-level discrete-time state-transition equations are established, and a next-generation matrix is constructed under age aggregation to analyze the epidemic threshold. Fourth, Monte Carlo simulations are conducted to quantitatively evaluate the effects of information-spreading strategies, initial information seed locations, and network structures on epidemic dynamics. The results provide a mechanism-level assessment of how age-dependent information diffusion and infection-induced feedback regulate infection peaks, information coverage, and epidemic evolution. In addition, empirical comparisons are performed using four types of real infectious disease data, including viral cold, influenza, acute intestinal infectious disease, and COVID-19, to qualitatively investigate the regulatory role of information diffusion in epidemic spreading processes.

2. Materials and Methods

2.1. Construction of the Information–Epidemic Coupled Spreading Model

In this study, a three-layer age-heterogeneous multilayer hypernetwork is used as the spreading carrier. Its topological structure and top-view projection are shown in Figure 1. The network divides the population into three mutually coupled subnetworks according to spreading behaviors and susceptibility characteristics, namely youth, middle-aged individuals, and older adults. Each layer follows connection rules according to its specific interaction mechanism, while interlayer coupling is established through household relationships. This hypernetwork can effectively describe the heterogeneity among different age groups in terms of information-spreading ability, social activity, and disease susceptibility. Meanwhile, through both intralayer and interlayer connection rules, it provides a network representation that is closer to complex interpersonal contact patterns in real society. Compared with traditional single-layer or two-layer networks, the age-heterogeneous multilayer hypernetwork can better reflect population differences and thus provides a more realistic network basis for the analysis of information–epidemic coupled spreading dynamics in this study.

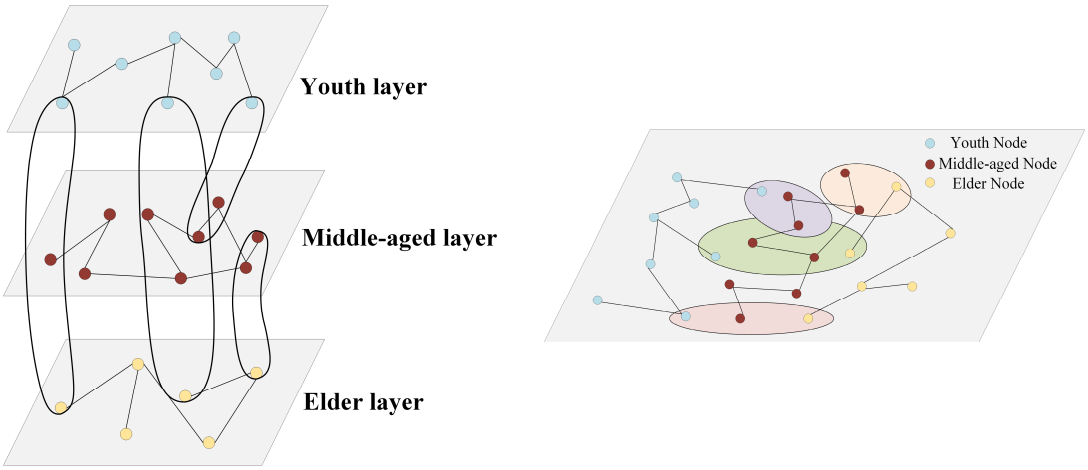


Figure 1. Age-family hyperedge multilayer heterogeneous network structure. (**a**) 3D schematic of the three-layer network with youth, middle-aged, and elderly age groups connected via household hyperedges; (**b**) Top view of the age-stratified multilayer network with household hypergroup clusters.

On the basis of the age-heterogeneous multilayer hypernetwork, and in response to the limitations of existing information–epidemic coupled models that do not sufficiently integrate age heterogeneity with information diffusion, this study constructs a four-layer information–epidemic coupled heterogeneous network. The network consists of one virtual information layer and three physical age-specific disease layers, including the youth layer, the middle-aged layer, and the older-adult layer. These layers are mutually coupled, and connections within each layer and household-based cross-age interactions follow heterogeneous construction rules. The schematic topology of the proposed network is shown in Figure 2. The virtual information layer is responsible for the diffusion of protective information and is not constrained by physical contact. Instead, it interacts with the age-specific disease layers through cross-layer node mapping. The youth, middle-aged, and older-adult layers serve as physical disease-spreading layers, where disease transmission occurs through interpersonal contacts. At the same time, nodes in these layers receive protective information from the virtual information layer through cross-layer connections, thereby enabling bidirectional coupled spreading between information diffusion and disease transmission.

Although different layers represent different interaction mechanisms, the coupling between layers is not established through arbitrary interlayer edges. Specifically, the virtual information layer and the physical disease layers share the same population node set through one-to-one node correspondence. Each individual node in the information layer corresponds to the identical individual node in the disease layers, and the information state of each node affects its disease transition probabilities through the coupled state-transition mechanism.

The virtual information layer is constructed according to information diffusion relationships, whereas the physical disease layers are generated according to age-dependent contact patterns. Therefore, the differences among layers originate from their interaction meanings and connection-generation rules rather than from independent populations. Household relationships are introduced as close-contact structures connecting individuals from different age groups. Individuals belonging to the same household are connected through household edges, which influence both disease transmission and information exchange among family members.

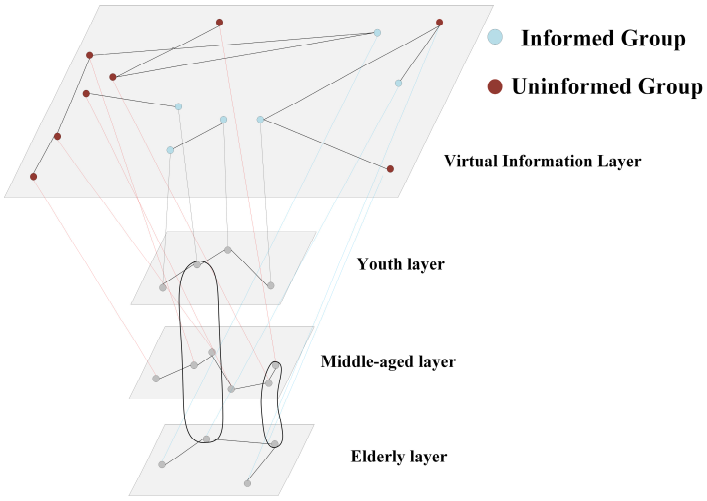


Figure 2. The four-layer information–disease-coupled heterogeneous mixed network proposed in this work, containing one virtual information layer and three age-based disease transmission layers (youth, middle-aged, elderly layers, with gray nodes representing individuals belonging to different age groups). Light blue nodes stand for informed individuals and dark red nodes stand for uninformed individuals in the information layer; straight lines between layers represent the coupling connections of information and disease spread. Each physical individual node in the three age layers has a one-to-one corresponding node in the virtual information layer, and the vertical connecting lines indicate the mapping relationship between physical nodes and information nodes.

For age-dependent contacts, the contact matrix Cab is used to characterize the average interaction intensity between individuals from age groups a and b. During the construction of the physical disease network, the probability of establishing a contact edge between two individuals is determined according to the corresponding element of Cab. Specifically,

$$P(A_{ij} = 1 \mid a_i = a, a_j = b) = C_{ab},$$

where A_{ij} denotes the adjacency relationship between individuals i and j. The same age-dependent contact structure is further used in the epidemic threshold analysis to construct the age-aggregated next-generation matrix.

The model is established based on the following assumptions: (1) individuals are mapped one-to-one between the information layer and the disease layer, although the connection-generation mechanisms of the two layers are different; (2) disease transmission occurs only in the physical contact network, whereas information diffusion occurs only in the information network; (3) individuals who are aware of protective information have a reduced infection risk and a higher probability of recovery or treatment compliance after infection; (4) the infected state increases individuals' willingness to disseminate protective information, thereby forming a feedback effect from disease transmission to information diffusion; and (5) specific pathogen types are not distinguished in this study, and the model parameters are represented as normalized probabilities, which can be calibrated using disease-specific data in future applications.

Age heterogeneity is a core setting of the proposed model. Youth groups usually exhibit strong peer clustering, and school-based and peer contacts play an important role in their disease transmission. Middle-aged individuals are involved in work, family, and social interactions, and therefore have more frequent cross-age contacts, potentially serving as an important bridge between the youth layer and the older-adult layer. Older adults generally have relatively stable contact ranges, but they may have higher infection risks and lower recovery capacity in certain disease scenarios. Age-related contact patterns have been widely confirmed by social contact surveys and contact matrix studies [15–17].

At the network generation level, this study allows different age layers to adopt different topological structures. If random and relatively homogeneous contacts need to be represented, an ER random network can be used. If heterogeneous social structures with hub nodes need to be described, a BA scale-free network can be adopted [18,19]. To represent strong ties such as household relationships, interlayer household edges or household hyperedges can be introduced among the three age layers. Household relationships usually involve frequent and close contacts; therefore, relatively high transmission weights can be assigned to these connections in the disease transmission layer [17–19].

After the network is constructed, spreading states are defined separately in the virtual information layer and the physical disease layers. Nodes in the information layer are classified into different states according to their awareness of epidemic prevention information, whereas nodes in the disease layers are classified as susceptible, infected, or recovered according to the disease progression process. On this basis, the cross-layer coupling mechanism enables information diffusion to indirectly regulate disease transmission. Specifically, after receiving and becoming aware of protective information, individuals may adopt preventive behaviors such as wearing masks, reducing gatherings, and undergoing active testing, thereby reducing the probability of disease transmission. Meanwhile, widely disseminated health information can also improve individuals' willingness to seek medical treatment and their treatment compliance, thereby indirectly increasing the recovery probability. Consequently, a coupled process is formed in which information diffusion and disease transmission interact with each other and coevolve dynamically.

The coupling between layers follows a one-to-one individual mapping and a state-oriented regulation rule. Each individual node exists simultaneously in the virtual information layer and in the corresponding age-specific physical disease layer, enabling cross-layer node correspondence. The epidemic prevention awareness state of an individual in the information layer dynamically modifies the transmission and recovery parameters of the corresponding node in the disease layer, thereby enabling active intervention in disease transmission. Conversely, the infection status in the disease layer also acts back on the information layer by increasing individuals' willingness to disseminate information and reducing information forgetting, thus changing the diffusion process of epidemic prevention information. These two processes interact and evolve dynamically, forming a bidirectional cross-layer coupling mechanism.

The four-layer mixed heterogeneous network constructed in this study separates the virtual layer of information diffusion from the physical layers of disease transmission, thereby reflecting the difference between contact-free information diffusion and contact-based disease transmission. In addition, by introducing three age-heterogeneous disease layers corresponding to youth, middle-aged individuals, and older adults, together with directed cross-layer coupling rules, the proposed topology captures the heterogeneity of different age groups in social behavior, information acquisition ability, and disease susceptibility. This topological structure provides a clear network basis for incorporating information-diffusion dynamics and deriving coupled state-transition equations. It also improves the applicability of the model to realistic scenarios and supports subsequent theoretical analysis of information–epidemic coupled spreading dynamics.

The main contributions of this paper are summarized as follows:

A UA-SIR age-heterogeneous multilayer network model is proposed to jointly describe information diffusion and epidemic spreading among youth, middle-aged, and elderly populations.

Age-dependent transmission parameters and household cross-age interactions are incorporated to capture heterogeneous behavioral characteristics.

A bidirectional coupling mechanism is introduced, where awareness suppresses disease transmission and infection promotes information diffusion.

An age-aggregated next-generation matrix is established to theoretically analyze the epidemic threshold, and extensive simulations together with real epidemic datasets are used to validate the proposed framework.

2.2. Definition of Spreading States and Rule Analysis

The state of each node is jointly determined by its information state and disease state. The information state includes the unaware state U and the aware state A. The unaware state indicates that an individual has not received or has not adopted relevant protective information, whereas the aware state indicates that an individual has acquired protective information and may adopt preventive behaviors, such as wearing masks, reducing gatherings, undergoing active testing, and seeking timely medical treatment. The disease state follows the SIR spreading framework, including the susceptible state S, infected state I, and recovered state R.

Therefore, the coupled state of node i at any time t can be represented by one of six combinations: US, UI, UR, AS, AI, and AR. For example, US indicates that the node is unaware of protective information and is susceptible; AI indicates that the node is aware of protective information but is still infected; and AR indicates that the node is aware of protective information and has recovered from the disease. Let $P_i^{\mathrm{US}}(t)$, $P_i^{\mathrm{UI}}(t)$, $P_i^{\mathrm{UR}}(t)$, $P_i^{\mathrm{AS}}(t)$, $P_i^{\mathrm{AI}}(t)$, and $P_i^{\mathrm{AR}}(t)$ denote the probabilities that node i is in the corresponding states at time t, respectively. In this study, one discrete simulation time step represents one unit of epidemic evolution time. For simplicity and consistency with the epidemic spreading literature, each time step is interpreted as one day. Therefore, the temporal evolution curves shown in the following experiments use days as the time unit. These probabilities satisfy the following normalization condition:

$$P_i^{\mathrm{US}}(t) + P_i^{\mathrm{UI}}(t) + P_i^{\mathrm{UR}}(t) + P_i^{\mathrm{AS}}(t) + P_i^{\mathrm{AI}}(t) + P_i^{\mathrm{AR}}(t) = 1 \tag{1}$$

For simplicity, the probability that node i is aware of protective information and the probability that node i is infected at time t are defined as follows:

$$P_i^{\mathrm{A}}(t) = P_i^{\mathrm{AS}}(t) + P_i^{\mathrm{AI}}(t) + P_i^{\mathrm{AR}}(t) \tag{2}$$

$$P_i^{\mathrm{I}}(t) = P_i^{\mathrm{UI}}(t) + P_i^{\mathrm{AI}}(t) \tag{3}$$

The model is based on the following basic assumptions. First, disease transmission occurs only in the physical disease layers, whereas information diffusion occurs only in the virtual information layer. Second, individuals who are aware of protective information adopt certain preventive behaviors, thereby reducing their probability of infection. Third, infected individuals who are aware of protective information have higher treatment compliance or a stronger willingness to seek medical care, and therefore their recovery probability is relatively increased. Fourth, the infected state enhances individuals' willingness to disseminate protective information, thereby forming a feedback effect from disease transmission to information diffusion. Fifth, recovered individuals no longer participate in the current round of disease transmission, and no transition from R back to S is considered.

The preceding section defines the coupled node states, the normalization constraint of state probabilities, and the key aggregated probabilities. Since the model involves a series of parameters and state probability symbols that distinguish information states, disease states, and age-stratified layers, this section summarizes the core variables and provides standardized definitions to ensure consistency throughout the paper and to help

readers quickly understand the physical meanings of the mathematical symbols, as shown in Table 1.

Table 1. Table of Core Symbols Used in the Model.

Symbol	Definition
$a \in \{y,m,e\}$	Age layer, representing youth, middle-aged individuals, and older adults, respectively
M_{ij}	Adjacency matrix of the virtual layer, namely the information layer, $M_{ij} = 1$ if node (i) is connected to node (j) in the information layer
B_{ij}	Adjacency matrix of the physical layer, namely the disease layer, $B_{ij} = 1$ if node (i) is connected to node (j) in the information layer
λ	Information-spreading rate, denoted by λ_y, λ_m, λ_e for different age layers; after infection, denoted by λ_i^A
δ	Information forgetting rate, denoted by δ_y, δ_m, δ_e for different age layers
α	Disease transmission rate, denoted by α_y, α_m, α_e for different age layers; after awareness, denoted by α_i^A
β	Disease recovery rate, denoted by β_y, β_m, β_e for different age layers; after awareness, denoted by β_i^{A}
$P_i^{\mathrm{US}}(t)$	Probability that node (i) is in the (US) state at time (t)
$P_i^{\mathrm{UI}}(t)$	Probability that node (i) is in the (UI) state at time (t)
$P_i^{\mathrm{UR}}(t)$	Probability that node (i) is in the (UR) state at time (t)
$P_i^{\mathrm{AS}}(t)$	Probability that node (i) is in the (AS) state at time (t)
$P_i^{\mathrm{AI}}(t)$	Probability that node (i) is in the (AI) state at time (t)
$P_i^{\mathrm{AR}}(t)$	Probability that node (i) is in the (AR) state at time (t)
$\mathrm{r}_i(t)$	Probability that node (i) is not informed by its neighbors in the virtual information layer at time (t)
$q_i^U(t)$	Probability that node (i), when unaware, is not infected by its neighbors in the physical disease layer at time (t)
$q_i^A(t)$	Probability that node (i), when aware, is not infected by its neighbors in the physical disease layer at time (t)
$\gamma, 0 < \gamma < 1$	Reduction rate of disease transmission after becoming aware of protective information
$\eta, 0 < \eta < 1$	Increase rate of disease recovery after becoming aware of protective information
$\omega, 0 < \omega < 1$	Increase rate of information-spreading after infection
C_{ab}	Contact intensity between infected individuals in age layer (a) and susceptible individuals in age layer (b)
K	Next-generation matrix
$\rho(K)$	Spectral radius of matrix (K), namely the maximum modulus of its eigenvalues

2.2.1. Information Diffusion Mechanism

Real-world social media platforms and online information diffusion networks usually exhibit significant degree heterogeneity, in which a small number of highly connected nodes play a key role in information dissemination. Therefore, this study adopts a BA scale-free network to represent the virtual information layer. Based on this topology, the

UA spreading model is used to describe the diffusion process of epidemic prevention information, where individuals' information states are divided into the unaware state U and the aware state A. Individuals in the unaware state have not acquired relevant epidemic prevention information, whereas individuals in the aware state have acquired such information and may adopt protective measures.

The information layer adopts the unaware–aware UA process to describe the diffusion of protective information. Nodes in the unaware state U can receive protective information from their neighbors in the information layer and transition to the aware state A. Nodes in the aware state A may forget the information and return to the unaware state U due to attention decay, information fatigue, or a decline in risk perception. Information-spreading rates and forgetting rates differ across age groups. In general, youth groups are more active in online social interactions and have a higher frequency of information exposure, but their information retention may be less stable. Middle-aged individuals have broader social connections and often act as information intermediaries in both household and workplace settings. Older adults have relatively limited information channels, and their efficiency in receiving and retaining information may be lower.

Within each time step, an unaware node can obtain protective information from its neighbors in the information layer and become aware. Meanwhile, an aware node may forget the information due to information fatigue, attention decay, or reduced risk perception, thereby returning to the unaware state. Considering age heterogeneity, different age layers are assigned different information-spreading rates λa and forgetting rates δa.

To account for the feedback effect of infection status on individuals' willingness to disseminate information, the effective information-spreading rate of node j at time t is defined as

$$\lambda_j^{eff}(t) = \min\{1, \lambda_a(j)[1+\omega P_j^I(t)]\} \tag{4}$$

where a(j) denotes the age layer to which node j belongs, $P_j^I(t)$ represents the probability that node j is in the infected state at time t, and ω is the infection-induced feedback coefficient. When $\omega = 0$, infection status has no effect on information diffusion. When $\omega > 0$, a higher infection probability indicates a stronger tendency of the node to disseminate protective information. The minimum function is used to ensure that the effective information-spreading rate does not exceed 1. The probability that node i does not receive protective information from any neighbor in the information layer at time t is given by

$$r_i(t) = \prod_{j=1}^{N}[1 - M_{ij}\lambda_j^{eff}(t)P_j^A(t)]. \tag{5}$$

Therefore, the probability that an unaware node i transitions to the aware state within one time step is $1 - r_i(t)$.

2.2.2. Disease Transmission Mechanism

In the simulation experiments, the disease layer adopts the SIR epidemic model to describe disease transmission. Nodes in the susceptible state S can be infected by infected neighbors in the disease layer and then transition to the infected state I. Nodes in the infected state I can recover with a certain probability and transition to the recovered state R. The recovered state R indicates that individuals no longer participate in the current round of disease transmission, and no transition from R back to S is considered in this study. Equation (6) describes the dynamic transition process among the three population groups, namely susceptible, infected, and recovered individuals, over time:

$$\begin{cases} \frac{dS}{dt} = -\alpha SI \\ \frac{dI}{dt} = \alpha SI - \beta I \\ \frac{dR}{dt} = \beta I \end{cases} \tag{6}$$

where α denotes the disease transmission rate, and β denotes the disease recovery rate. The classical SIR model described by the above differential equations provides the fundamental mechanism of epidemic transmission in a homogeneous population. However, the objective of this study is to investigate the co-evolution of awareness diffusion and epidemic spreading on age-heterogeneous multilayer networks. To facilitate node-level stochastic state transitions and Monte Carlo simulations, the proposed UA–SIR model is formulated in a discrete-time Markov framework, in which all node states are synchronously updated at each discrete time step. Therefore, the continuous-time SIR equations presented above are introduced only as theoretical background and are not used in the derivation of the proposed model.

2.2.3. Information–Epidemic Coupling Relationship

There is a bidirectional coupling relationship between information diffusion and disease transmission. When individuals receive and become aware of epidemic prevention information, they may adopt protective behaviors, such as wearing masks and reducing gatherings, timely medical treatment and medication compliance, thereby reducing the probability of disease transmission and improving recovery efficiency. Importantly, this improved recovery efficiency reflects enhanced behavioral treatment adherence and voluntary isolation, rather than accelerated intrinsic physiological healing of the disease itself. In this way, information diffusion actively intervenes in the disease transmission process, as shown in Equations (7)–(9). Meanwhile, the health risks caused by disease transmission can stimulate the public to actively acquire and disseminate epidemic prevention information, further promoting information diffusion. Once disease transmission begins, infected individuals tend to have a stronger willingness to disseminate epidemic prevention information, and the information-spreading rate of a node increases with its infection status, as shown in Equation (9). Therefore, disease transmission accelerates the diffusion of epidemic prevention information, while information diffusion in turn constrains disease spread. These two processes interact with each other and form a dynamic feedback mechanism, reflecting the coevolutionary relationship between infectious diseases and epidemic prevention information in realistic scenarios.

$$\partial_i^A = \min\{1, (1-\gamma)\partial_i\}, 0 < \partial_i^A \leq 1 \tag{7}$$

$$\beta_i^A = \min\{1, (1+\eta)\beta_i\}, 0 < \beta_i^A \leq 1 \tag{8}$$

$$\lambda_a^I = \min\{1, (1+\omega)\lambda_a\}, 0 < \lambda_a^I \leq 1 \tag{9}$$

where α_i^A denotes the disease transmission rate of individual i when in the aware state A, α_i denotes the initial disease transmission rate of individual i, β_i^A denotes the disease recovery rate of individual i when in the aware state A, β_i denotes the initial disease recovery rate of individual i, λ_i^I denotes the information-spreading rate of individual i when in the infected state I, and λ_i denotes the initial information-spreading rate of individual i. The parameter γ represents the transmission reduction coefficient under the aware state, η represents the recovery enhancement coefficient under the aware state, and ω represents the promotion coefficient of infection status on information-spreading. This setting indicates that individuals who are aware of protective information are more likely to reduce their effective infectious duration in the spreading network by adopting behaviors such as active testing, timely medical treatment, home isolation, proper medication, and

reduced secondary exposure. It should be noted that awareness does not directly change an individual's physiological recovery capacity.

If node i is connected to several infected neighbors in the disease layer, the probability that it is not infected can be approximated under the assumption of independent transmission from neighboring nodes. If the updated information state of node i in the current time step is U, the probability that it remains uninfected is given by

$$q_i^U(t) = \prod_{j=1}^{N}[1 - B_{ij}\alpha_a^U(i)P_j^I(t)] \quad (10)$$

If the updated information state of node (i) in the current time step is (A), the probability that it remains uninfected is given by

$$q_i^A(t) = \prod_{j=1}^{N}[1 - B_{ij}\alpha_a^A(i)P_j^I(t)] \quad (11)$$

Therefore, under the information state $X \in \{U,A\}$, the probability that node i transitions from the susceptible state S to the infected state I is $1 - q_i^X(t)$. If the edges in the disease layer have different contact intensities, B_{ij} can be replaced by a weighted matrix W_{ij}, resulting in a more general weighted transmission form. It should be noted that the network generation probability p_a is only used to generate the ER network or to set the average connection density. It should not be multiplied again with the number of existing infected neighbors; otherwise, the transmission probability would be counted repeatedly.

Based on the four-layer multilayer coupled network and the bidirectional coupling mechanism described above, this study develops a UA-SIR information–epidemic coupled spreading model. The overall operating logic and key procedures of the model are shown in Figure 3. The flowchart presents the complete process from topology construction, layer-specific spreading, cross-layer coupling, and node state evolution to simulation updating and result analysis. It also illustrates the bidirectional coupling pathways between the information layer and the disease layers, the differentiated setting of age-heterogeneous parameters, and the state transition rules, thereby providing a clear logical basis for the subsequent derivation of dynamical equations and simulation experiments.

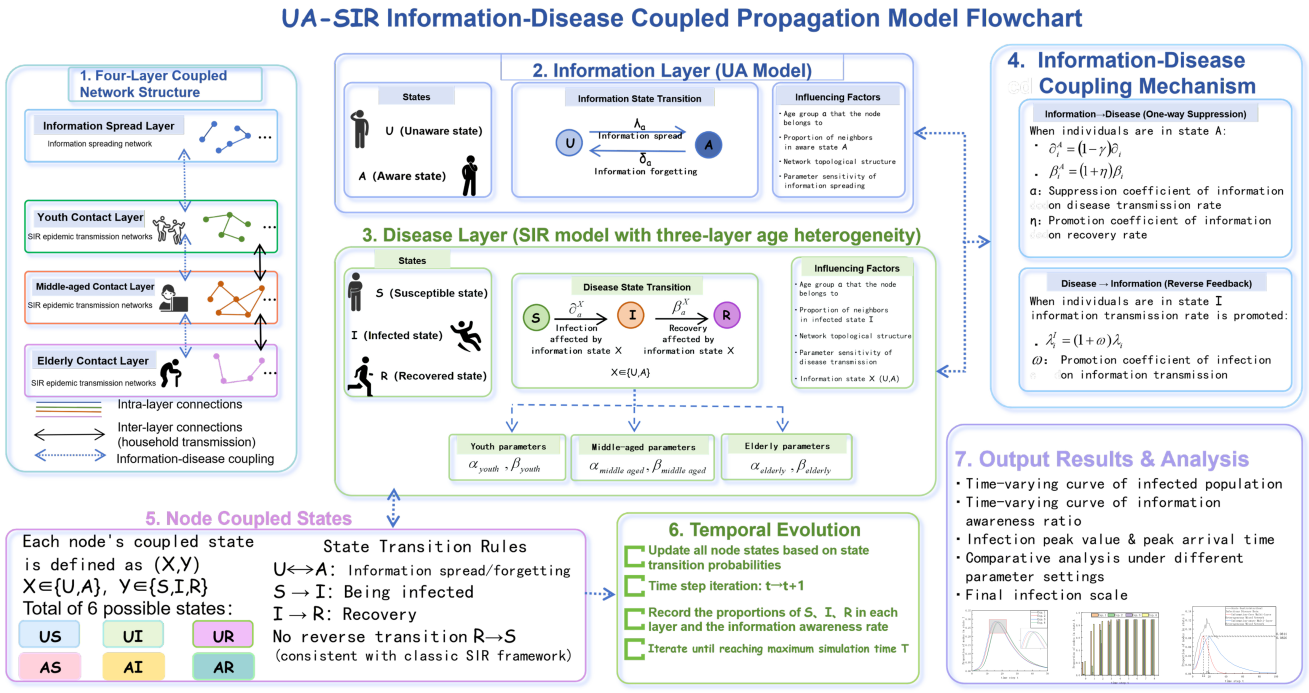


Figure 3. UA-SIR Information-Disease Coupled Propagation Model Flowchart.

3. Node State Transitions and Dynamical Equations

3.1. State Transition Rules

In the discrete-time framework, the transition of node states from time t to time $t + 1$ is jointly determined by the transition of the information state and the transition of the disease state. This study adopts a stepwise discrete-time updating rule. Within each time step, the information state of each node is first updated according to the states of its neighbors in the information layer. Then, based on the updated information state, the disease transmission and recovery probabilities are modified, and the SIR state update is completed in the disease layer.

The transition probabilities of the information state are defined as follows:

$$Pr(U \to U) = r_i(t),\ Pr(U \to A) = 1 - r_i(t) \tag{12}$$

$$Pr(A \to U) = \delta_{a_i},\ Pr(A \to A) = 1 - \delta_{a_i} \tag{13}$$

The transition probabilities of the disease state depend on the current information state $X \in \{U,A\}$ of the node. If X = U, $q_i^U(t)$ and β_a^U are used; if X = A, $q_i^A(t)$ and β_a^A are used. The disease state transition probabilities are given as follows:

$$Pr(S \to S|X) = q_i^X(t),\ Pr(S \to I|X) = 1 - q_i^X(t) \tag{14}$$

$$Pr(I \to I|X) = 1 - \gamma_a^X,\ Pr(I \to R|X) = \gamma_a^X \tag{15}$$

$$Pr(R \to R|X) = 1 \tag{16}$$

where X denotes the information state of the node at time (t). According to the above rules, the transition probability from any coupled state (X,D) to (X',D') can be written as the product of the information state transition probability and the disease state transition probability:

$$Pr\left[(X,D) \to (X',D')\right] = Pr(X \to X')Pr(D \to D'|X') \tag{17}$$

where X and X' denote the information states before and after updating, respectively, and D and D' denote the disease states before and after updating, respectively. This expression emphasizes that the disease state transition probability depends on the updated information state X'. Therefore, it can cover all possible transition pathways among the six coupled states US, UI, UR, AS, AI, and AR.

3.2. State Transition Tree

To intuitively illustrate the state evolution paths and transition probabilities of nodes during the information–epidemic coupled spreading process, this section constructs a coupled state-transition tree, as shown in Figure 4. The coupled state of a node is formed by combining its information state, namely the unaware state U or the aware state A, with its disease state, namely the susceptible state S, infected state I, or recovered state R. Accordingly, six basic coupled states are obtained: US, UI, UR, AS, AI, and AR.

The state transition tree takes each basic state as a root node and hierarchically presents all possible evolution paths of a node under the effects of information diffusion, disease infection, recovery, and information forgetting. The corresponding transition probabilities are also marked in the tree, including the information acquisition probability $1 - r_i(t)$, the information forgetting probability δi, the disease infection probabilities $1 - q_i{}^A(t)$ and $1 - q_i{}^U(t)$, and the disease recovery probabilities $\beta_i{}^A$ and $\beta_i{}^U$, which depend on the current information state of the node.

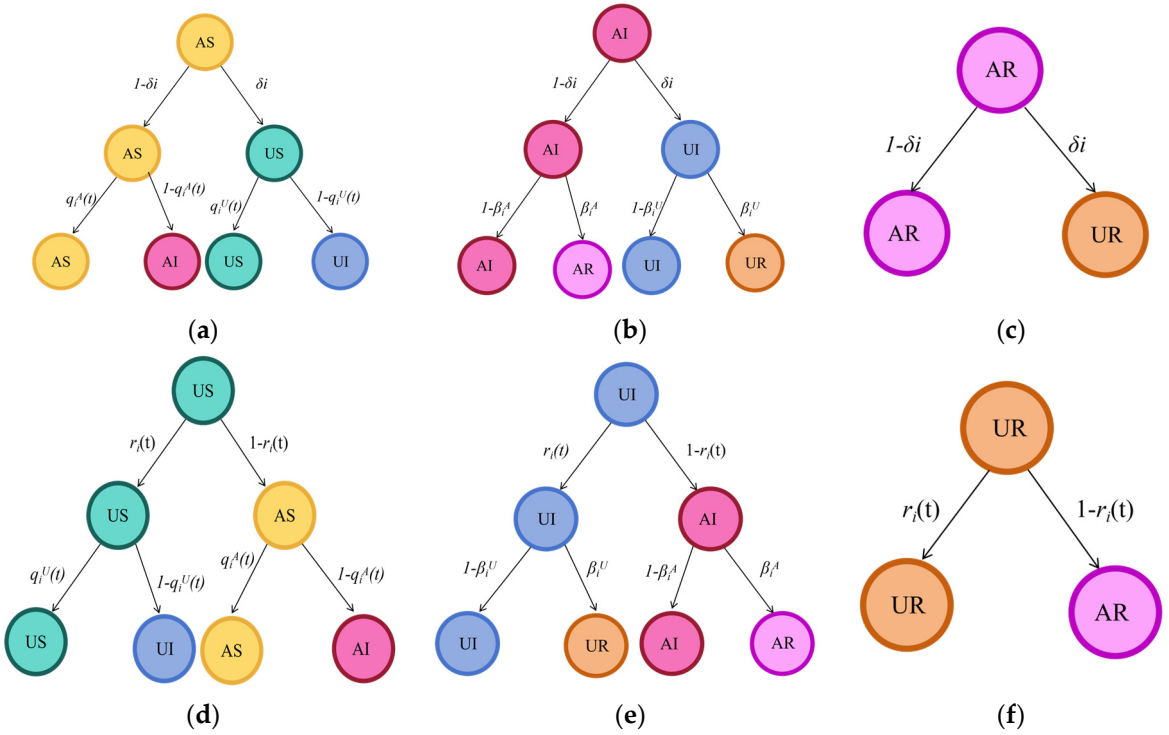


Figure 4. State transition probability tree. Panels (**a**–**f**) show the transition paths starting from the six coupled states (AS), (AI), (AR), (US), (UI), and (UR), respectively. The transition probabilities include information acquisition $1 - r_i(t)$, information forgetting δi, disease infection $1 - q_i{}^A(t)$ or $1 - q_i{}^U(t)$, and recovery $\beta_i{}^U$ or $\beta_i{}^A$, depending on the information and disease states of the node.

The state transition tree clearly characterizes the dynamic evolution logic of node states under the bidirectional coupling mechanism. On the one hand, changes in the information state affect the probability of disease infection through the two branches $q_i{}^U(t)$ and $q_i{}^A(t)$. On the other hand, the disease infection state also influences the information diffusion and forgetting behaviors of nodes. Based on this state transition tree, the probability expressions of each coupled state at the next time step can be derived, thereby providing intuitive logical support for the subsequent construction of the complete coupled state transition equations.

3.3. Properties of the Proposed State Transition Model

To establish the mathematical consistency of the proposed UA–SIR model, we prove that the six-state transition system preserves the probability simplex. Specifically, the following proposition demonstrates that the total probability remains normalized and that all state probabilities remain non-negative throughout the evolution process.

Proposition 1. *For every node* i, *assume that the initial state probabilities satisfy:* $p_i^s(0) \geq 0$, $\forall s \in \Omega$, *and* $\sum_{s\in\Omega} p_i^s(0) = 1$, *where the set of coupled states is* $\Omega = \{US, UI, UR, AS, AI, AR\}$.

If all state-transition probabilities belong to the interval [0, 1], then the six-state transition Equations (18)–(23) preserve both probability normalization and non-negativity for every $t \geq 0$.

Proof. Define the state-probability vector of node i at time t as

$$\boldsymbol{p}_i(t) = \left(p_i^{\mathrm{US}}(t), p_i^{\mathrm{UI}}(t), p_i^{\mathrm{UR}}(t), p_i^{\mathrm{AS}}(t), p_i^{\mathrm{AI}}(t), p_i^{\mathrm{AR}}(t)\right)^T.$$

The six state-transition equations can be expressed in matrix form as $\boldsymbol{p}_i(t+1) = \boldsymbol{T}_i(t)\boldsymbol{p}_i(t)$, where $\boldsymbol{T_i}(t)$ denotes the time-dependent state-transition matrix of node i. Under the parameter constraints $0 \le r_i(t) \le 1, 0 \le q_i^U(t) \le 1, 0 \le q_i^A(t) \le 1$, and $0 \le \delta_i \le 1, 0 \le \beta_i^U \le 1$, $0 \le \beta_i^A \le 1$, all entries of $\boldsymbol{T_i}(t)$ are non-negative. For each current coupled state, all possible states at the next time step are mutually exclusive and collectively exhaustive. Therefore, the transition probabilities from each current state sum to one, $\sum_{s' \in \Omega} [\boldsymbol{T}_i(t)]_{s',s} = 1, \forall s \in \Omega$.

Thus, $\mathbf{T_i}$(t) is a column-stochastic matrix. Let $\boldsymbol{e} = (1,1,1,1,1,1)^T$. It follows that

$$\sum_{s\in\Omega} p_i^s(t+1) = \boldsymbol{e}^T \boldsymbol{p}_i(t+1) = \boldsymbol{e}^T \boldsymbol{T}_i(t)\boldsymbol{p}_i(t) = \boldsymbol{e}^T \boldsymbol{p}_i(t) = \sum_{s\in\Omega} p_i^s(t).$$

Since $\sum_{s\in\Omega} p_i^s(0) = 1$, it follows by mathematical induction that $\sum_{s\in\Omega} p_i^s(t) = 1, \forall t \ge 0$. Furthermore, because $\boldsymbol{T_i}(t) \ge 0$ and $\boldsymbol{p}_i(t) \ge \mathbf{0}$, we obtain $\boldsymbol{p}_i(t+1) = \boldsymbol{T}_i(t)\boldsymbol{p}_i(t) \ge \mathbf{0}$.

Therefore, $p_i^s(t) \ge 0, \forall s \in \Omega, \forall t \ge 0$.

Hence, the proposed six-state UA–SIR transition equations preserve both probability normalization and non-negativity. □

3.4. State Transition Equations

According to the above transition rules, the six-state probability evolution equations of node i can be obtained, as shown in Equations (18)–(23)

$$p_i^{\mathrm{US}}(t+1) \quad = r_i(t) q_i^U(t) p_i^{\mathrm{US}}(t) + \delta_i q_i^U(t) p_i^{\mathrm{AS}}(t) \ , \tag{18}$$

$$\begin{aligned} p_i^{\mathrm{UI}}(t+1) = {} & r_i(t)\left(1-\beta_i^U\right) p_i^{\mathrm{UI}}(t) + r_i(t)\left(1-q_i^U(t)\right) p_i^{\mathrm{US}}(t) \\ & + \delta_i\left(1-\beta_i^U\right) p_i^{\mathrm{AI}}(t) + \delta_i\left(1-q_i^U(t)\right) p_i^{\mathrm{AS}}(t), \end{aligned} \tag{19}$$

$$\begin{aligned} p_i^{\mathrm{UR}}(t+1) = {} & r_i(t)\beta_i^U p_i^{\mathrm{UI}}(t) + \delta_i \beta_i^U p_i^{\mathrm{AI}}(t) \\ & + r_i(t) p_i^{\mathrm{UR}}(t) + \delta_i p_i^{\mathrm{AR}}(t), \end{aligned} \tag{20}$$

$$p_i^{\mathrm{AS}}(t+1) = (1-r_i(t)) q_i^A(t) p_i^{\mathrm{US}}(t) + (1-\delta_i) q_i^A(t) p_i^{\mathrm{AS}}(t), \tag{21}$$

$$\begin{aligned} p_i^{\mathrm{AI}}(t+1) = {} & (1-r_i(t))\left(1-q_i^A(t)\right) p_i^{\mathrm{US}}(t) + (1-\delta_i)\left(1-\beta_i^A\right) p_i^{\mathrm{AI}}(t) \\ & + (1-r_i(t))\left(1-\beta_i^A\right) p_i^{\mathrm{UI}}(t) + (1-\delta_i)\left(1-q_i^A(t)\right) p_i^{\mathrm{AS}}(t), \end{aligned} \tag{22}$$

$$\begin{aligned} p_i^{\mathrm{AR}}(t+1) = {} & (1-r_i(t))\beta_i^A p_i^{\mathrm{UI}}(t) + (1-\delta_i)\beta_i^A p_i^{\mathrm{AI}}(t) \\ & + (1-\delta_i) p_i^{\mathrm{AR}}(t) + (1-r_i(t)) p_i^{\mathrm{UR}}(t), \end{aligned} \tag{23}$$

The above equations fully describe the state evolution of nodes under the bidirectional coupling mechanism, where $r_i(t)$, $q_i^U(t)$, and $q_i^A(t)$ denote the probabilities related to information diffusion and disease infection derived in the previous section. δ_i represents the information forgetting rate, while ${\beta_i}^U$ and ${\beta_i}^A$ denote the disease recovery rates under different information states. This system of equations provides the core dynamical model for the subsequent simulation experiments.

3.5. Matrix Form and Macroscopic Indicators

The state probability vector of node (i) is defined as

$$p_i(t) = \left[P_i^{\mathrm{US}}(t), P_i^{\mathrm{AS}}(t), P_i^{\mathrm{UI}}(t), P_i^{\mathrm{AI}}(t), P_i^{\mathrm{UR}}(t), P_i^{\mathrm{AR}}(t)\right] \tag{24}$$

Then, the state evolution of the node can be written as

$$p_i(t+1) = p_i(t) T_i(t) \tag{25}$$

where $T_i(t)$ is a non-homogeneous state transition matrix jointly determined by $r_i(t)$, $q_i^U(t)$, $q_i^A(t)$, δa, β_a^A, and β_a^U. Since $r_i(t)$, $q_i^U(t)$, and $q_i^A(t)$ dynamically change with the states of

other nodes in the network, the transition matrix is generally time-varying. Therefore, the proposed process can be regarded as a discrete-time non-homogeneous Markov process.

To describe the overall spreading dynamics of the system, the global information awareness rate $A(t)$, infection proportion $I(t)$, and recovery proportion $R(t)$ are defined as follows:

$$A(t) = N^{-1} \sum_{i=1}^{N} P_i^A(t) \tag{26}$$

$$I(t) = N^{-1} \sum_{i=1}^{N} P_i^I(t) \tag{27}$$

$$R(t) = N^{-1} \sum_{i=1}^{N} [P_i^{UR}(t) + P_i^{AR}(t)] \tag{28}$$

3.6. Age-Aggregated Epidemic Threshold Analysis

3.6.1. Linearization near the Disease-Free Equilibrium

The epidemic threshold is used to determine whether a small number of infected individuals introduced into the system can trigger large-scale spreading. A rigorous threshold analysis usually requires linearizing the infection variables near the disease-free equilibrium and constructing a next-generation matrix. For the age-heterogeneous information–epidemic coupled model proposed in this study, node states are simultaneously affected by information states, disease states, and age-layer structures. Therefore, the epidemic threshold cannot be simply expressed as the ratio between a single infection rate and a recovery rate.

The disease-free equilibrium is defined as the state in which there are no infected individuals in the system, that is, for all nodes: $P_i^I(t) = 0$.

At this point, only the information diffusion process evolves independently, and an age-specific steady-state awareness proportion ρ_a^A can be formed.

At the early stage of disease invasion, the infection proportion is very low, and it can be approximated as

$$P_i^I(t) \approx 0,\ S_i(t) \approx 1 \tag{29}$$

Under this condition, the feedback term from infection status to information diffusion does not directly enter the epidemic threshold under the first-order linear approximation, because

$$\lambda_j^{eff}(t) \ = \lambda_a(j)[1+\omega P_j^I(t)] \ \approx \lambda_a(j) \tag{30}$$

This indicates that, under a given awareness structure or the quasi-steady state of information diffusion at the disease-free equilibrium, the infection-induced feedback term ω does not directly contribute to the first-order linear invasion term of the infection variables. Therefore, ω does not explicitly appear in the threshold expression in this study. However, ω can still affect the infection peak, peak time, and final infection size by accelerating information diffusion during the spreading process.

To obtain an analytically tractable and epidemiologically interpretable epidemic threshold, we linearize the age-aggregated infection subsystem around the disease-free equilibrium and construct an age-aggregated next-generation matrix. Since the proposed UA-SIR model contains six coupled node states on a multilayer age-heterogeneous network, the complete node-level linearization would lead to a 6N $\times$ 6N Jacobian matrix, which is analytically intractable and difficult to interpret. Therefore, following the common practice in multilayer epidemic modeling, this study derives the epidemic threshold from an age-aggregated infection subsystem. The resulting next-generation matrix provides an interpretable approximation of the early-stage invasion dynamics under the disease-free equilibrium rather than an exact node-level threshold. Let ρ_a^A denote the proportion of individuals who are aware of protective information in age layer a during the early stage

of disease invasion. The value of ρ_a^A can be determined by the initial information seed structure or by the quasi-steady awareness proportion formed by the information diffusion process under the disease-free state.

3.6.2. Effective Infection Rate and Effective Recovery Rate of Age Layers

Given the awareness proportion ρ_a^A in age layer a, the average effective infection rate of individuals in this age layer can be expressed as the weighted average of the infection rate in the unaware state and that in the aware state: $\overline{\alpha_a} = (1 - \rho_a^A)\alpha_a^U + \rho_a^A\alpha_a^A$.

If $\alpha_a^A = (1 - \gamma)\alpha_a^U$ is adopted, then $\overline{\alpha_a} = (1 - \gamma\rho_a^A)\alpha_a^U$.

Similarly, the average effective recovery rate of individuals in age layer a is given by $\overline{\beta_a} = (1 - \rho_a^A)\beta_a^U + \rho_a^A\beta_a^A$.

If $\beta_a^A = (1 + \eta)\beta_a^U$ is adopted, then $\overline{\beta_a} = (1 + \eta\rho_a^A)\beta_a^U$.

Thus, a higher awareness proportion ρ_a^A in an age layer leads to a lower effective infection rate and a higher effective recovery rate, thereby reducing the risk of disease transmission.

3.6.3. Construction of the Next-Generation Matrix

Based on the linearized age-aggregated infection subsystem, let C_{ab} denote the average intensity of effective contacts per unit time between infected individuals in age layer a and susceptible individuals in age layer b. Here, a represents the age layer of the infection source, while b represents the age layer of the susceptible individuals being infected. The element K_{ba} of the next-generation matrix represents the expected number of new infections in age layer b caused by a single infected individual from age layer a during the entire infectious period. Therefore, the expected number of new infections in age layer b caused by one infected individual from age layer a can be expressed as

$$K_{ba} = C_{ab} \cdot \overline{\alpha_b} / \overline{\beta_a}.$$

where $\overline{\beta_a}$ is the average effective recovery rate of the infection source in age layer a, and $1/\overline{\beta_a}$ represents the average infectious duration of the infected individual. $\overline{\alpha_b}$ is the average effective infection rate of susceptible individuals in age layer b, representing the probability of infection per effective contact.

For the three age layers, namely youth, middle-aged individuals, and older adults, a 3×3 next-generation infection matrix $K = [K_{ba}]$ is constructed. The columns of the matrix correspond to the age layer a of the infection source, and the rows correspond to the infected age layer b, where $a, b \in \{y, m, e\}$.

It should be noted that C_{ab} in this study is defined as the average intensity of effective contacts per unit time between a single infected individual in age layer a and susceptible individuals in age layer b. Therefore, no additional correction term for age-layer population proportions is introduced when constructing the next-generation matrix. If C_{ab} is derived from a reciprocal contact matrix obtained from real social contact surveys, whether a population-size correction should be included needs to be further determined according to the definition of the contact matrix.

3.6.4. Threshold Criterion

Based on the next-generation matrix, the effective basic reproduction number of the age-heterogeneous information–epidemic coupled system under a given awareness structure is defined as

$$R_0^{eff} = \rho(K).$$

where $\rho(K)$ denotes the spectral radius of matrix K, namely the maximum modulus of its eigenvalues. The threshold criterion is given as follows:

$R_0^{eff} < 1$: the disease cannot persistently spread in the system, and the infection size tends to decline;

$R_0^{eff} > 1$: the disease has the potential to invade and spread, and the system faces an outbreak risk.

It should be emphasized that the proposed threshold is an age-aggregated approximation of the early-stage invasion dynamics rather than the exact epidemic threshold derived from the full node-level Jacobian. Nevertheless, it captures the dominant effects of age-specific contacts, awareness-dependent transmission, and recovery processes while maintaining analytical tractability and epidemiological interpretability. It is more appropriate than a simple ratio of the average infection rate to the recovery rate, because it simultaneously considers the age-specific contact structure C_{ab}, the awareness proportion ρ_a^A of each age layer, the inhibitory effect of information on the infection rate, and the promoting effect of information on the recovery rate.

It should be emphasized that R_0^{eff} mainly characterizes the linear spreading risk at the early stage of disease invasion, whereas the infection-induced feedback mechanism ω primarily affects the nonlinear dynamics in the middle and late stages of spreading. Therefore, in the subsequent simulation experiments, R_0^{eff} can be reported together with Monte Carlo simulation indicators, such as the infection peak, peak time, and final infection size, to verify the consistency between the threshold indicator and the actual spreading outcomes. Future work will investigate the exact node-level epidemic threshold by performing a full Jacobian-based stability analysis for the proposed six-state age-heterogeneous multilayer network.

4. Multidimensional Simulation Experiments and Result Analysis

Each experimental setting was independently simulated 50 times, and the reported curves represent the corresponding mean values. The time-dependent standard deviations of the principal experiment are presented in Section 4.1, while those of the additional structural sensitivity analyses are provided in Supplementary Material.

Numerical simulation calculations were coded with Python 3.9 (Python Software Foundation, Wilmington, DE, USA). All curves and figures in this manuscript were drawn and polished using Origin 2021 (OriginLab Corporation, Northampton, MA, USA).

4.1. Parameter Setting and Comparative Analysis of Each Group

To verify the effects of age-specific information diffusion strategies and infection-induced feedback mechanisms on the information diffusion process, this study sets up three experimental scenarios: Control Group A, Control Group B, and the experimental group. Control Group A adopts a unified information-spreading rate and forgetting rate, without distinguishing differences in information diffusion among youth, middle-aged individuals, and older adults. Control Group B introduces age-specific information-spreading rates and forgetting rates, but does not consider the feedback effect of infection status on information-diffusion behavior. On the basis of age-specific parameter settings, the experimental group further introduces an infection-induced enhancement mechanism for information-spreading, indicating that infected individuals are more likely to actively disseminate protective information due to increased risk perception.

As shown in Table 2, the reduction rate of disease transmission after awareness, γ, and the enhancement rate of disease recovery after awareness, η, are kept consistent across the three groups and are both set to 0.5. Therefore, the differences among the three groups mainly arise from the age heterogeneity of information diffusion parameters and

the introduction of the infection feedback mechanism ω. This setting makes it possible to separately examine the influence of changes in the information diffusion mechanism on the overall spreading process while keeping the inhibitory effect of awareness on disease transmission unchanged.

Table 2. Comparative Experiment Between the Experimental Group and Control Groups.

Parameters		Control Group A	Control Group B	Experimental Group
Information transmission rate	Youth	0.183	0.25	0.25
	Middle-aged	0.183	0.18	0.18
	Elderly	0.183	0.12	0.12
Information forgetting rate	Youth	0.15	0.15	0.15
	Middle-aged	0.15	0.1	0.1
	Elderly	0.15	0.2	0.2
Reduction rate of disease transmission rate after information awareness γ		0.5	0.5	0.5
Promotion rate of disease recovery rate after information awareness η		0.5	0.5	0.5
Promotion rate of information transmission rate after disease infection ω		-	-	0.5

To construct a neutral homogeneous baseline, the information transmission and forgetting rates in Control Group A are set to the arithmetic means of the corresponding age-specific parameters in the experimental group. This preserves the overall parameter magnitude while eliminating age heterogeneity, ensuring a balanced comparison.

Unless otherwise stated, the parameter values are selected according to representative settings reported in previous epidemic modeling studies and are used to investigate the coupled spreading mechanism rather than to calibrate a specific infectious disease. To further evaluate the robustness of the model under different parameter settings, sensitivity analyses are conducted by varying key parameters, including information-spreading rates, forgetting rates, network size, average degree, and household coupling strength. The results indicate that the main qualitative conclusions remain consistent under different parameter configurations.

As shown in Figure 5a, the information awareness rates of all three groups increase rapidly in the early stage and reach relatively high levels within a short period, indicating that protective information can diffuse quickly in the information layer. In Control Group A, the awareness rate increases relatively slowly because unified information diffusion parameters are used. After age-specific spreading parameters are introduced in Control Group B, the information diffusion speed increases, suggesting that considering differences in information-spreading ability and forgetting characteristics among different age groups helps improve overall information coverage more rapidly. The experimental group shows the fastest increase in awareness rate during the early stage and maintains a relatively high level in the later stage, indicating that the infection feedback mechanism can further promote the diffusion of protective information. When individuals become infected, their risk perception increases, which enhances their willingness to disseminate protective information and enables more nodes to acquire such information during the early stage of disease transmission. As shown in Figure 6a, the standard deviation of the aware-state proportion is relatively large during the initial information-diffusion stage, especially within the first several time steps, and then decreases rapidly. Although the experimental

group exhibits a slightly larger initial fluctuation because of the infection-induced feedback mechanism, the standard deviations of all three groups soon converge to a relatively low level, approximately between 0.002 and 0.004. This result indicates that the awareness dynamics are more sensitive to stochastic initial conditions and local network structure during the early diffusion stage, whereas the information-coverage process becomes highly stable after approaching its steady state.

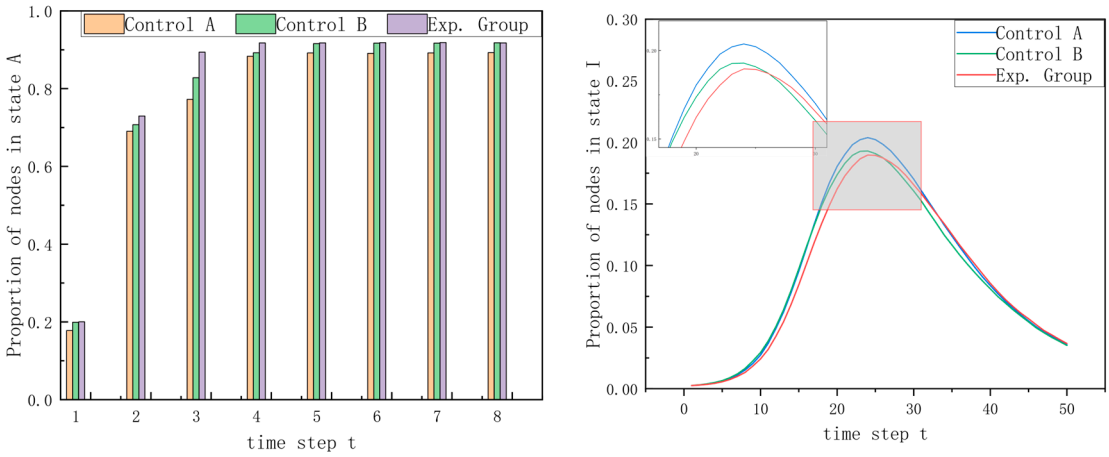


Figure 5. Comparison between the experimental group and the control groups. (**a**) Partial view of the information awareness rate ($A(t)$) over time (day). Only the early and middle stages are shown because the awareness rate changes only slightly after reaching a relatively stable level in the later stage. (**b**) Evolution curves of the infection proportion ($I(t)$) in the disease transmission process. Control A adopts unified information diffusion parameters, Control B introduces age-specific information diffusion parameters, and the experimental group further incorporates the infection-induced feedback mechanism.

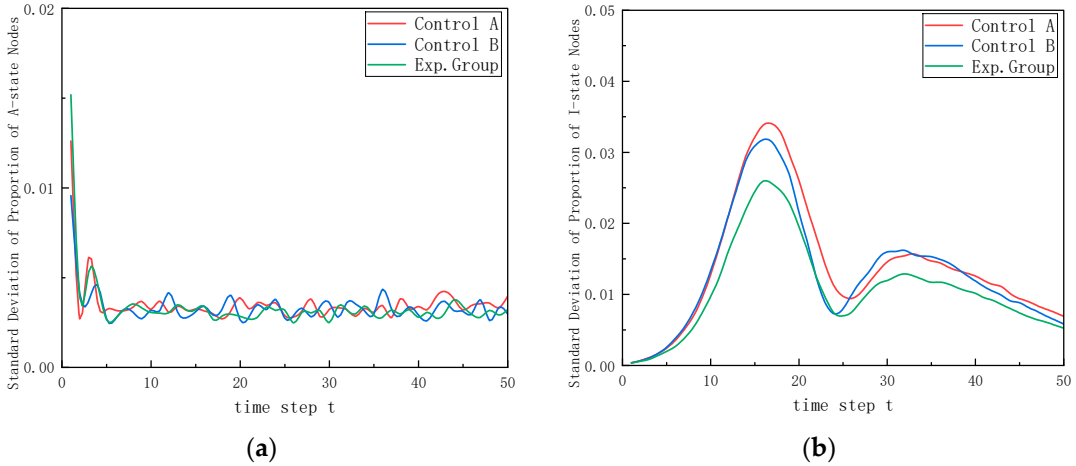


Figure 6. Stochastic variability of the coupled spreading dynamics. (**a**) Standard deviation of the aware proportion; (**b**) Standard deviation of the infected proportion. The standard deviations were calculated from 50 independent Monte Carlo realizations.

As shown in Figure 5b, the infection proportion I(t) in all three groups exhibits typical SIR dynamics, characterized by an initial increase, a peak, and a subsequent decline. However, differences can still be observed in the infection peaks and curve shapes among the groups. Control Group A has the highest infection peak, indicating that under unified information diffusion parameters, information diffusion fails to sufficiently reflect differences among age groups, and its inhibitory effect on disease transmission is relatively limited. In

Control Group B, after age-specific information diffusion parameters are introduced, the infection peak decreases slightly, suggesting that assigning different information-spreading rates and forgetting rates to different age groups can improve the diffusion efficiency of protective information to some extent and thereby reduce disease transmission intensity. The experimental group has the lowest infection peak, and its infection curve is generally lower than those of the two control groups. This indicates that introducing the infection feedback mechanism on the basis of age-specific information diffusion can further enhance the inhibitory effect of information diffusion on disease transmission. Figure 6b further presents the standard deviations of the infected-state proportion obtained from 50 independent Monte Carlo simulations. The standard-deviation curves exhibit two distinct fluctuation peaks. The first and largest peak occurs at approximately the 17th–18th time step, corresponding to the rapid epidemic-development stage, whereas a smaller second peak appears around the 30th–33rd time step. These peaks indicate that stochastic differences among independent realizations are most pronounced during the epidemic growth and transition stages. Control Group A generally exhibits the largest variability, followed by Control Group B, while the experimental group shows the lowest standard deviation over most of the simulation period. In particular, the maximum standard deviation decreases from approximately 0.034 in Control Group A to approximately 0.026 in the experimental group. This suggests that the age-specific information parameters and infection-induced feedback mechanism reduce not only the mean infection prevalence but also the run-to-run variability of the epidemic process. After the second fluctuation peak, the standard deviations gradually decrease in all three groups, indicating increasing convergence among independent realizations during the epidemic-decay stage.

By jointly analyzing the changes in information awareness rate and infection proportion, it can be found that higher information diffusion efficiency is generally associated with a lower infection peak. In the experimental group, a high level of information coverage is formed more rapidly during the early stage of spreading, allowing more susceptible individuals to acquire protective information in advance and adopt corresponding preventive behaviors, thereby reducing their probability of infection. Meanwhile, the infection feedback mechanism enables infected nodes to further promote the diffusion of protective information, forming a dynamic feedback process of "disease transmission–enhanced risk perception–accelerated information diffusion–suppressed disease transmission". Therefore, compared with Control Group A and Control Group B, the experimental group exhibits a stronger inhibitory effect on disease spreading.

It should be noted that the differences among the three infection curves are not drastic, but are mainly reflected in the gradual reduction in the infection peak and overall curve height. This indicates that, under the current parameter settings, age-specific information diffusion strategies and the infection feedback mechanism have a certain inhibitory effect on disease transmission, although the magnitude of this effect is jointly constrained by factors such as the baseline disease transmission rate, information diffusion efficiency, and information forgetting rate. This result suggests that relying solely on a unified information diffusion strategy may not fully exploit the role of protective information. In contrast, incorporating age-group differences and infection-induced feedback can more reasonably characterize the coupling relationship between information diffusion and disease transmission in real public health events.

In summary, the comparative results between the experimental group and the control groups show that age-specific information diffusion strategies can improve the diffusion efficiency of protective information, while the infection feedback mechanism can further enhance the dynamic responsiveness of information diffusion. Under their combined effect, the infection peak is reduced to some extent, and the spreading process is

moderately suppressed. These results validate the rationality of introducing age heterogeneity and infection-induced feedback into the proposed information–epidemic coupled spreading model.

4.2. Sensitivity Analysis of the Information-Spreading Rate λ and Forgetting Rate δ

To analyze the effects of the information-spreading rate and information forgetting rate on the information–epidemic coupled spreading process, as shown in Table 3, this study takes Experiment 1 as the baseline group. Under the condition that other parameters remain unchanged, the information-spreading rate λ and information forgetting rate δ of the youth, middle-aged, and older-adult layers are adjusted separately, and Experiments 2–8 are designed for comparative analysis. While Figure 6a shows the corresponding changes in the information awareness rate $A(t)$ during information diffusion, Figure 6b shows the changes in the infection proportion $I(t)$ during disease transmission under different experimental conditions.

Table 3. Parameter settings for the sensitivity analysis of age-specific information-spreading and forgetting rates.

Parameter Sensitivity Analysis 1		Exp.1	Exp.2	Exp.3	Exp.4	Exp.5	Exp.6	Exp.7	Exp.8
Information transmission rate	λ_y	0.25	0.3	0.4	0.25	0.25	0.25	0.25	0.25
	λ_m	0.18	0.18	0.18	0.25	0.18	0.18	0.18	0.18
	λ_e	0.12	0.12	0.12	0.12	0.18	0.12	0.12	0.12
Information forgetting rate	δ_y	0.15	0.15	0.15	0.15	0.15	0.25	0.15	0.15
	δ_m	0.1	0.1	0.1	0.1	0.1	0.1	0.2	0.1
	δ_e	0.2	0.2	0.2	0.2	0.2	0.2	0.2	0.3

From the perspective of the information awareness rate, the awareness rate of each experimental group gradually increases over time and tends to remain at a relatively high level in the later stage. This indicates that protective information can continuously diffuse in the information layer and form broad information coverage. However, certain differences can still be observed among the experimental groups in terms of early information diffusion speed and final awareness level. In Experiment 2, the information-spreading rate of the youth layer, λ_y, is slightly increased compared with that in Experiment 1. However, the improvement in the awareness rate is not obvious, and its effect on the infection curve is also weak. This suggests that a small increase in the information-spreading rate of the youth layer is insufficient to significantly change the overall spreading process. In Experiment 3, after the information-spreading rate of the youth layer is further increased, the information diffusion speed is enhanced, and the infection peak is relatively reduced. This indicates that when the information-spreading ability of the youth layer reaches a certain level, it can strengthen the diffusion of protective information within the youth group and its adjacent groups, thereby exerting a more noticeable inhibitory effect on disease transmission.

In Experiment 4, the information-spreading rate of the middle-aged layer, λ_m, is increased. The awareness rate increases more rapidly in the early stage, indicating that stronger information-spreading ability in the middle-aged layer enables protective information to diffuse more effectively to other age layers. In age-heterogeneous networks, middle-aged individuals usually serve as a bridge connecting the youth layer, the older-adult layer, and broader social contacts. Therefore, improving the information-spreading ability of this layer is more likely to affect the global information coverage level and further change the disease transmission process. In Experiment 5, the information-spreading rate of the older-adult layer, λ_e, is increased. From the awareness curve, this adjustment improves the overall information coverage to a certain extent, but its effect on the infection

peak is relatively limited. This suggests that increasing the information-spreading rate of the older-adult layer can improve information diffusion within the older-adult group, but due to its relatively weaker cross-layer connectivity, its regulatory effect on global disease transmission is less obvious than that of the youth and middle-aged layers.

From the perspective of information forgetting rate, Experiments 6, 7, and 8 increase the information forgetting rates of the youth, middle-aged, and older-adult layers, respectively. Compared with the baseline experiment, an increase in the information forgetting rate weakens individuals' ability to continuously retain protective information, causing some nodes to return to the unaware state and thereby reducing the inhibitory effect of information diffusion on disease transmission. In particular, after the forgetting rate of the middle-aged layer is increased in Experiment 7, the peak of the awareness rate decreases significantly, while the infection peak increases noticeably. This indicates that the information retention ability of the middle-aged layer plays an important role in the overall prevention and control effect of the system. Since the middle-aged layer has strong cross-age connections and acts as an information intermediary, an increase in its forgetting rate weakens both the continuous diffusion of protective information within the network and its cross-layer transmission, which further increases infection risk. In Experiments 6 and 8, increasing the forgetting rates of the youth and older-adult layers also changes the infection curves to some extent, but the overall effect is weaker than that caused by changes in the forgetting rate of the middle-aged layer.

Overall, Figure 7 shows that the information-spreading rate and forgetting rate further affect the infection proportion by changing the rising speed and stable level of the information awareness rate. In general, a faster increase in the awareness rate and a higher awareness level in the later stage are more conducive to reducing the infection peak and flattening the infection curve. Conversely, an increase in the information forgetting rate weakens the protective effect of information, leading to a higher infection peak or a prolonged spreading process. These results indicate that the role of protective information in disease transmission depends not only on whether information can diffuse rapidly, but also on whether individuals can continuously retain protective awareness.

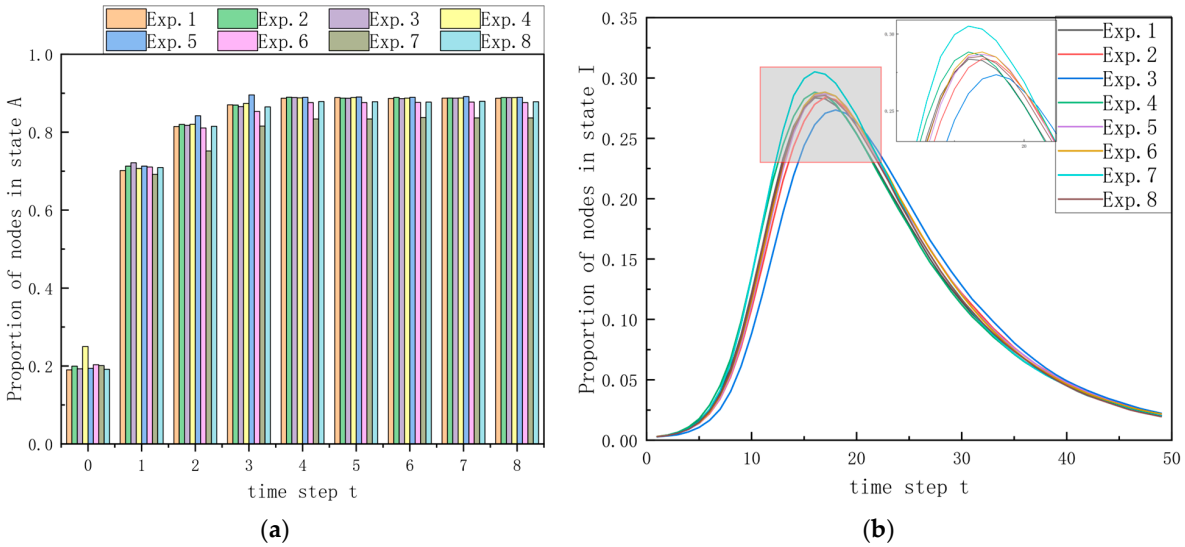
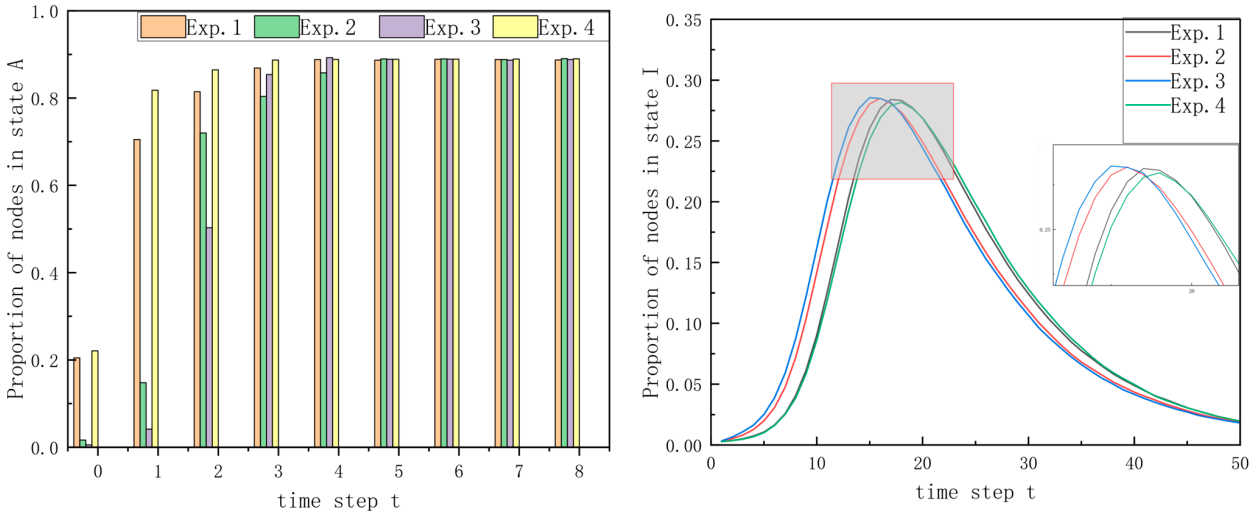


Figure 7. Sensitivity analysis of the information-spreading rate λ and forgetting rate δ. (**a**) Partial view of the information awareness rate ($A(t)$) under different parameter settings. Only the early and middle stages are shown because the curves change only slightly after reaching a relatively stable level in the later stage. (**b**) Evolution curves of the infection proportion ($I(t)$) in the disease transmission process under different parameter settings. Experiments 1–8 correspond to different adjustments of the information-spreading rate and forgetting rate in the youth, middle-aged, and older-adult layers.

4.3. Sensitivity Analysis of Initial Information Seed Locations

To analyze the effect of the initial information seed location on the information–epidemic coupled spreading process, this study sets up four comparative experiments. In Experiment 1, the initial information seeds are placed in the middle-aged layer; in Experiment 2, they are placed in the youth layer; in Experiment 3, they are placed in the older-adult layer; and in Experiment 4, they are allocated according to the age proportions. Under the condition that the network structure, disease transmission parameters, information-spreading rates, information forgetting rates, and the inhibitory parameters of information on disease transmission remain unchanged, the changing trends of the information awareness proportion (A(t)) and the infection proportion (I(t)) under different initial information seed locations are compared.

As shown in Figure 8a, the results of the information awareness proportion (A(t)) indicate that the initial information seed location has a noticeable effect on the speed of information diffusion. The awareness proportions of all four experiments eventually reach relatively high levels, suggesting that protective information can spread widely in the information layer under the given information-spreading and forgetting rates. However, in the early stage of spreading, the information diffusion speed varies significantly across different seed locations. The mixed seeding group shows the fastest increase in the awareness proportion and reaches a relatively high level within a short time, indicating that allocating initial information seeds according to age proportions allows protective information to enter multiple age layers simultaneously, thereby improving early information coverage. The middle-aged seeding group also shows a relatively fast information diffusion speed, suggesting that the middle-aged layer has strong cross-layer connectivity and an information intermediary role, enabling it to effectively promote information diffusion toward both the youth and older-adult layers. In contrast, when seeds are placed only in the youth layer or the older-adult layer, the early diffusion of information to other age layers is relatively slow, indicating that seeding in a single age layer is more likely to be constrained by intralayer spreading range and cross-layer connectivity.



(**a**) (**b**)

Figure 8. Sensitivity analysis of initial information seed locations. (**a**) Partial view of the information awareness rate ($A(t)$) under different initial information seed locations. Only the early and middle stages are shown because the curves change only slightly after reaching a relatively stable level in the later stage. (**b**) Evolution curves of the infection proportion ($I(t)$) in the disease transmission process under different seed-location strategies. Experiments 1–4 correspond to information seeds initially placed in the middle-aged layer, youth layer, older-adult layer, and mixed-age layers, respectively.

As shown in Figure 8b, the results of the infection proportion (I(t)) show that different initial information seed locations also affect the disease transmission process. The infection curves of all four groups exhibit typical SIR spreading characteristics, with an initial increase, a peak, and a subsequent decline. However, differences can be observed in the rising speed and peak time. The infection curves of the older-adult and youth seeding groups rise more rapidly in the early stage and reach their peaks relatively earlier, indicating that when protective information is mainly concentrated in a single age layer, it is difficult for information to promptly cover groups with frequent cross-age contacts, and disease transmission may still spread rapidly in the early stage. By contrast, the infection curves of the middle-aged seeding group and the mixed seeding group increase more gradually, and their peak times are relatively delayed. This suggests that placing information seeds in groups with strong cross-layer connectivity, or distributing seeds across multiple age layers simultaneously, is more conducive to forming an early population-level protective barrier and delaying the disease transmission process.

A further comparison between the information awareness proportion and the infection proportion shows that scenarios with faster information diffusion generally exhibit a slower increase in the infection curve and a shift in the infection peak occurrence toward later simulation time steps compared with the corresponding baseline scenarios. This indicates that initial information seeds affect not only the diffusion process within the information layer, but also the transmission dynamics in the disease layer through the cross-layer coupling mechanism. When protective information can cover key nodes and cross-layer connecting nodes earlier, more susceptible individuals can acquire protective information at the early stage of disease transmission, thereby reducing the effective infection probability and delaying the rapid growth of the infection size.

Overall, the results of the four experiments show that the initial information seed location has an important influence on both information diffusion efficiency and the tempo of disease transmission. The mixed seeding strategy can establish information sources simultaneously in multiple age layers and therefore performs well in improving the information awareness proportion. The middle-aged seeding strategy, relying on the strong cross-layer connectivity of middle-aged individuals, also shows a favorable effect in delaying disease transmission. In contrast, seeding only in the youth layer or the older-adult layer results in a relatively limited information diffusion range and a weaker inhibitory effect on global disease transmission. These results indicate that, in an age-heterogeneous multilayer network, public health information intervention should focus not only on the number of information seeds but also on their initial locations. Prioritizing middle-aged nodes with strong cross-age connectivity or adopting a mixed seeding strategy covering multiple age layers can help improve the diffusion efficiency of protective information and enhance its inhibitory effect on disease transmission.

4.4. Sensitivity Analysis of Network Topology

To analyze the effects of different network topologies on the information–epidemic coupled spreading process, this study sets up three comparative experiments. In Experiment 1, the youth, middle-aged, and older-adult layers all adopt BA scale-free networks. In Experiment 2, all three layers adopt ER random networks. In Experiment 3, the youth and middle-aged layers adopt BA scale-free networks, whereas the older-adult layer adopts an ER random network, forming a mixed topological structure. In the three experiments, the network size, initial infection proportion, information diffusion parameters, disease transmission parameters, and coupling parameters describing the effect of information on disease transmission are kept consistent. Only the topology of the disease transmission

layers is changed, so as to examine the influence of network structural differences on information diffusion and disease transmission.

As shown in Figure 9a, the changes in the infection proportion (I(t)) indicate that the disease transmission process differs substantially under different network topologies. When all three layers adopt ER random networks, the infection curve rises the fastest and reaches the highest peak at an earlier time, with a peak value significantly higher than those of the BA network and the mixed network. This suggests that in ER random networks, node connections are relatively homogeneous, allowing the disease to spread rapidly to a large number of nodes and making a concentrated outbreak more likely within a short period. Since ER networks lack obvious hub nodes, protective information can still diffuse, but it is difficult to form efficient transmission blocking through key nodes. As a result, the intensity of disease transmission is relatively high.

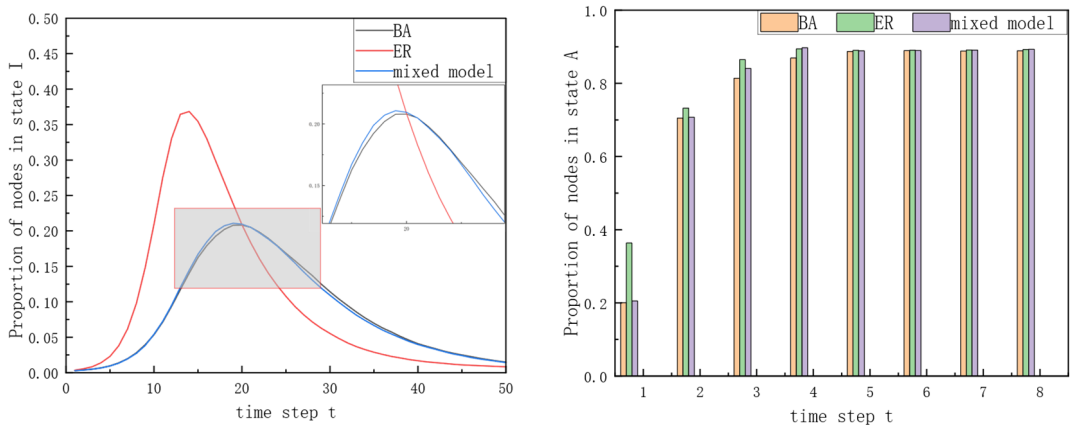


Figure 9. Sensitivity analysis of network topology. (**a**) Evolution curves of the infection proportion (I(t)) in the disease transmission process under different network topologies. (**b**) Partial view of the information awareness rate (A(t)) under different network topologies. Only the early and middle stages are shown because the curves change only slightly after reaching a relatively stable level in the later stage. BA denotes the case in which all three age layers adopt BA scale-free networks, ER denotes the case in which all three age layers adopt ER random networks, and the mixed model denotes the case in which the youth and middle-aged layers adopt BA networks while the older-adult layer adopts an ER network.

Compared with the ER random network, when all three layers adopt BA scale-free networks, the infection curve increases more slowly, the infection peak is substantially reduced, and the occurrence time of the infection peak shifts to a later simulation time step. This result indicates that, under the information–epidemic coupling mechanism proposed in this study, hub nodes in BA networks may serve not only as important pathways for disease transmission but also as key nodes for the rapid diffusion of protective information. When hub nodes acquire protective information at an early stage, their information-spreading ability and behavioral responses can affect a large number of adjacent nodes, thereby accelerating protective information coverage and weakening the ability of the disease to spread along core connection pathways. Therefore, under coupled information diffusion and disease transmission, BA networks exhibit stronger information diffusion advantages and protective blocking effects.

The infection curve of the mixed-topology network is relatively close to that of the BA scale-free network. The differences in peak height and peak time between the two are small, and both are clearly lower than those of the ER random network. This indicates that, after the youth and middle-aged layers adopt BA structures, the system still retains

strong hub-driven spreading characteristics. High-degree nodes in the youth and middle-aged groups can promote the diffusion of protective information and further suppress disease transmission. Since the older-adult layer adopts an ER random network, the mixed structure shows slight differences from the pure BA structure during some periods. However, its overall spreading trend remains close to that of the BA network, suggesting that the topological structures of the youth and middle-aged layers play a more important regulatory role in the overall spreading process.

As shown in Figure 9b, the changes in the information awareness proportion (A(t)) show that the awareness rate increases rapidly in the early stage and reaches a relatively high level within a short time under all three network topologies. This indicates that, under the given information diffusion parameters, protective information can spread widely across different topological structures. The awareness rate of the ER network is slightly higher in the early stage, but its infection peak remains the highest. This suggests that the speed of information coverage alone cannot fully determine the prevention and control effect; the influence of network structure on disease transmission pathways is equally important. Although the final awareness levels of the BA network and the mixed network are close to that of the ER network, their hub nodes play a key role in both information diffusion and disease transmission blocking. Therefore, their infection peaks are lower, and the spreading process is smoother.

Overall, network topology has a significant influence on information–epidemic coupled spreading. In ER random networks, node connections are relatively homogeneous, and disease transmission is more likely to form a rapid and concentrated outbreak. In BA scale-free networks, due to the existence of hub nodes, protective information can be diffused more effectively, and disease transmission pathways can be blocked more efficiently when information diffusion plays a sufficient role. The mixed topology combines the information diffusion advantages of BA networks with age-layer heterogeneity. Its spreading results are close to those of the pure BA network, while it is also more consistent with the real-world characteristics that youth and middle-aged groups usually have more active social connections, whereas older adults have relatively stable contact ranges. Therefore, in the subsequent empirical fitting, it is reasonable to adopt a mixed topology in which the youth and middle-aged layers are modeled as BA networks and the older-adult layer is modeled as an ER network.

5. Qualitative Comparison with Empirical Epidemic Trajectories

The empirical epidemic datasets used in this section are not employed for parameter calibration, optimization, or prediction evaluation. Instead, they serve as qualitative reference trajectories to examine whether the proposed information–epidemic coupling mechanism can reproduce general epidemic characteristics and illustrate the regulatory effect of information diffusion on disease transmission. Therefore, the comparison focuses on differences between epidemic dynamics with and without information diffusion under fixed representative parameter settings rather than disease-specific curve fitting.

To verify the applicability of the proposed information–epidemic coupled multilayer network model in real infectious disease spreading scenarios, this study selects four types of real infectious disease data for empirical experiments, namely viral cold, influenza, acute intestinal infectious disease, and COVID-19. The experiments compare the real infection proportion curves, the age-heterogeneous disease spreading model without information coupling, and the information–epidemic coupled multilayer network model with the information diffusion mechanism. The evaluation indicators mainly include the infection peak, peak time, peak error, peak-time error, and peak reduction rate, which are used to analyze the effects of information diffusion on disease spreading intensity and spreading

tempo. The real disease data are used to qualitatively verify the general epidemic evolution trend under fixed representative parameters, rather than for parameter calibration or precise time-series prediction. This study mainly focuses on the dynamic mechanism of information intervention and theoretical threshold analysis, while disease-specific model calibration will be explored in future work.

From the overall trend, all four types of real data exhibit a typical spreading process in which the infection proportion first increases, reaches a peak, and then gradually declines. The age-heterogeneous disease spreading model without information coupling can reasonably capture the basic spreading pattern of diseases in age-stratified contact networks. In particular, in spreading scenarios with relatively high peaks and concentrated outbreaks, such as viral cold, influenza, and COVID-19, the infection peaks generated by the model are relatively close to those of the real data. This indicates that the age-heterogeneous contact structure can, to some extent, reflect population contact differences in real disease transmission.

A further comparison between the model with information coupling and the model without information coupling shows that, after introducing the information diffusion mechanism, the infection curves generally exhibit reduced peaks, delayed peak times, and smoother curve shapes. This result indicates that the role of protective information is not simply to improve the point-by-point comparison accuracy of the model to the real curves. Instead, it changes the dynamic pattern of disease transmission by reducing the infection risk of aware individuals, increasing the effective recovery probability of infected individuals, and incorporating the feedback effect of infection status on information diffusion. As a result, an originally concentrated outbreak process is transformed into a lower-intensity but longer-lasting spreading process.

As shown in Figure 10a, for the viral cold data, the real infection curve is characterized by a rapid increase, a relatively high peak, and a rapid decline after the peak. The model without information coupling reproduces the general epidemic trend, including the approximate peak position and peak height of the real data. In contrast, the model with information coupling generates a lower infection peak than the model without information coupling, and the occurrence time of the infection peak shifts to a later simulation time step. This indicates that, under a high-transmission-intensity scenario, the diffusion of protective information can effectively reduce the short-term infection peak, but it may also lead to a certain low-level tailing phenomenon in the spreading process. This result reflects the "peak-shaving and curve-flattening" effect of information intervention.

As shown in Figure 10b, for the influenza data, the real curve also exhibits a high peak and rapid spreading characteristics. The model without information coupling can reasonably describe the concentrated outbreak trend of influenza, whereas the model with information coupling shows a lower infection peak and a smoother declining process than the model without information coupling. This suggests that, for respiratory infectious diseases with rapid transmission and large infection scales, the information diffusion mechanism can significantly weaken the intensity of concentrated outbreaks and delay the disease transmission process.

As shown in Figure 10c, for the acute intestinal infectious disease data, the overall real infection proportion is relatively low, and the spreading process is comparatively smooth. Compared with diseases with high transmission intensity, acute intestinal infectious disease does not form an obvious large-scale outbreak even in the model without information coupling. Therefore, after introducing the information diffusion mechanism, the decrease in the infection peak is not highly significant, and the effect is mainly reflected in the smoothing of the spreading process and changes in peak time. This indicates that the effect of information intervention varies across disease types. When the intrinsic transmission

intensity of a disease is relatively low, the inhibitory effect of the information mechanism is relatively limited, and its role is mainly reflected in regulating the spreading tempo rather than significantly reducing the infection peak.

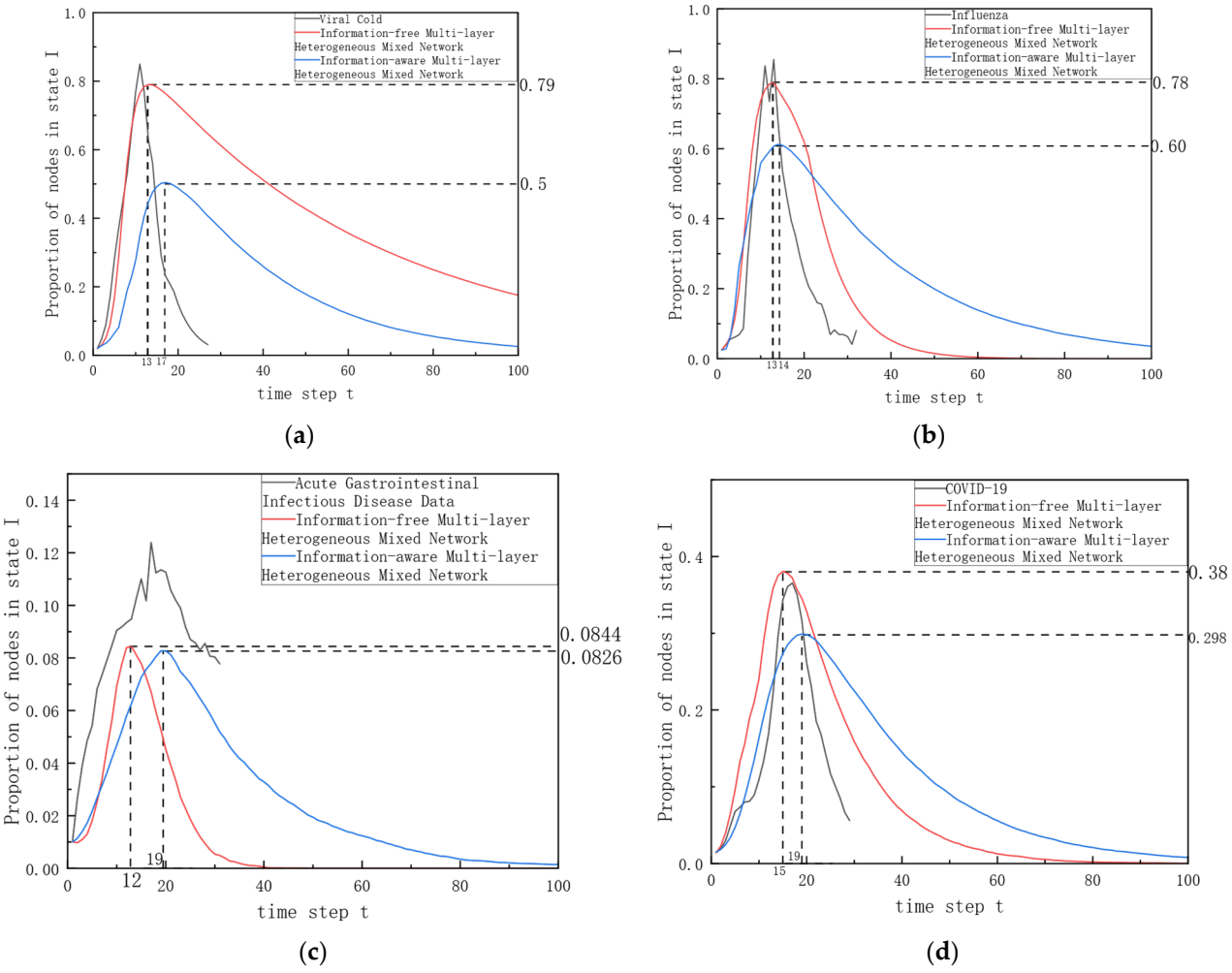


Figure 10. Empirical comparison of infection dynamics under different disease scenarios. (**a**) Viral cold; (**b**) influenza; (**c**) acute gastrointestinal infectious disease; (**d**) COVID-19. In each panel, the real infection data are compared with the information-free age-heterogeneous multilayer disease spreading model and the information-aware multilayer heterogeneous mixed network model. The dashed lines indicate the corresponding infection peaks and peak times. The results illustrate the effects of information diffusion on reducing the infection peak, delaying the peak time, and smoothing the epidemic spreading process under different types of infectious diseases.

As shown in Figure 10d, for the COVID-19 data, the real curve shows a rapid increase in the middle stage, followed by a relatively high peak and a gradual decline. The model without information coupling can reasonably approximate the peak height of the real curve, whereas the infection peak of the model with information coupling is clearly lower than that of the model without information coupling. Its infection peak occurs at a later simulation time step, and the overall curve becomes smoother. This indicates that, in medium- to high-intensity epidemic spreading scenarios, the information diffusion mechanism can produce obvious peak-reduction and delay effects on disease transmission by changing individual protective behaviors.

Overall, the empirical results of the four diseases show that the age-heterogeneous model without information coupling is more suitable for describing the basic spreading process under conditions where information intervention is not considered, whereas the

information–epidemic coupled model is more suitable for analyzing changes in the spreading process after protective information intervention is introduced. From the perspectives of infection peak, peak time, and spreading control effect, the model with information coupling more clearly reflects the regulatory effect of protective information on disease transmission. Specifically, it shows reduced infection peaks, shifts in the infection peak occurrence toward later simulation time steps, and smoother spreading curves, indicating that information diffusion can exert varying degrees of inhibitory effects on disease transmission under different disease scenarios.

Therefore, the empirical results demonstrate that the information–epidemic coupled multilayer network model constructed in this study can not only describe disease transmission under age-heterogeneous contact structures, but also further reveal the effects of protective information diffusion on disease transmission intensity and spreading tempo. These results validate the rationality of introducing the information diffusion mechanism into an age-heterogeneous multilayer disease transmission model. They also indicate that, in public health prevention and control, improving public awareness of protective information, enhancing information diffusion efficiency, and reducing information forgetting can help reduce infection peaks, delay disease spread, and alleviate short-term prevention and control pressure.

6. Conclusions

This study develops an information–epidemic coupled spreading model on an age-heterogeneous multilayer network by integrating protective information diffusion and epidemic transmission into a unified UA–SIR framework. By coupling a virtual information layer with three age-specific disease layers, the proposed model characterizes the heterogeneity of different age groups in information diffusion, contact behavior, infection risk, and recovery processes. Moreover, the model incorporates the effects of protective information on disease transmission, recovery enhancement, and infection-induced feedback on information-spreading. Compared with conventional information–epidemic models that usually assume homogeneous information diffusion or neglect the feedback between epidemic states and individual behaviors, the proposed framework provides a more detailed description of the dynamic interaction between information diffusion and epidemic transmission. The advantages of the proposed model are quantitatively reflected through changes in infection peaks, information coverage, and epidemic evolution under different intervention scenarios. These results demonstrate that incorporating age-dependent information diffusion and infection-induced feedback can improve the representation of behavioral heterogeneity and enhance the understanding of information-mediated epidemic regulation.

Theoretical analysis demonstrates that the epidemic threshold is jointly affected by age-dependent contact patterns, disease-related parameters, and information awareness levels. Increasing the proportion of informed individuals can reduce the effective infection rate and enhance the effective recovery rate, thereby lowering epidemic risks. Simulation results further show that age-specific information diffusion strategies and infection feedback mechanisms improve information-spreading efficiency and suppress disease transmission to varying degrees. Sensitivity analyses indicate that the middle-aged group plays an important role in information dissemination due to its relatively strong connectivity and information retention capability. Meanwhile, initial seeding strategies involving middle-aged individuals or mixed age groups can accelerate early information coverage and contribute to epidemic mitigation.

The empirical comparisons further demonstrate that introducing the information diffusion mechanism generally leads to lower infection peaks, smoother epidemic evolution,

and shifts in infection peak occurrence toward later simulation time steps in some scenarios. These results suggest that protective information is not merely an external intervention factor but can dynamically regulate epidemic evolution by influencing individual protective behaviors and recovery-related processes.

From a practical perspective, the finding that middle-aged or mixed seeding strategies improve information diffusion efficiency does not imply that elderly populations should be excluded from public health interventions. In real-world epidemic prevention, vaccination and awareness campaigns usually involve multiple objectives, including protecting vulnerable groups, reducing severe outcomes, and interrupting transmission chains. Therefore, effective intervention strategies should balance risk-oriented protection for vulnerable populations with information diffusion-oriented targeting of socially active groups.

Nevertheless, several limitations remain. The current model is based on abstract age structures and network assumptions and does not fully incorporate real individual contact networks. In addition, the awareness state is simplified into binary aware and unaware states without considering information credibility, behavioral adoption intensity, or heterogeneous protective responses. Furthermore, the empirical experiments mainly focus on qualitative comparisons rather than disease-specific prediction or parameter calibration. Future work will incorporate real contact matrices, time-varying networks, media-driven information diffusion, and more detailed behavioral mechanisms. Moreover, the current model assumes that infection enhances individuals' willingness to disseminate protective information, while severe symptoms may reduce communication ability and social activity. Incorporating disease severity and activity-dependent information diffusion behaviors will further improve the realism of the proposed framework.

Supplementary Materials: The following supporting information can be downloaded at: https://www.mdpi.com/article/10.3390/math14152746/s1, Figure S1: Mean spreading dynamics under different network sizes; Figure S2: Temporal variability under different network sizes; Figure S3: Mean spreading dynamics under different target average degrees; Figure S4: Standard deviations of the spreading states under different target average degrees; Figure S5: Mean spreading dynamics under different household transmission probabilities; Figure S6: Standard deviations of the spreading states under different household transmission probabilities.

Author Contributions: Conceptualization, Z.L. and X.M.; methodology, Z.L., X.M. and L.W.; software, F.M.; validation, F.M. and L.W.; formal analysis, F.M.; visualization, F.M. and L.W.; writing—original draft preparation, F.M. and Z.L.; writing—review and editing, X.M., X.Y. and L.W.; supervision, X.M. and X.Y. All authors have read and agreed to the published version of the manuscript.

Funding: This work was supported by two grants: the National Natural Science Foundation of China (Grant No. 62466049), titled "Data-driven Modeling and Characteristic Analysis of Individual-Based Multi-Pathogen Transmission Supernetworks", and the Natural Science Foundation of Qinghai Province (Grant No. 2025-ZJ-720), titled "Robustness of Multilayer Supernetworks and Its Application in the Sanjiangyuan Ecosystem".

Data Availability Statement: The datasets used in this study are publicly available as follows: 1. Data from the *National Statistical Yearbook 2024* are available at: https://www.stats.gov.cn/sj/ndsj/2024/indexch.htm (accessed on 20 December 2025). 2. The empirical experimental dataset is available from the Hong Kong Open Data Portal at: https://data.gov.hk/sc-datasets/category/health (accessed on 18 December 2025).

Acknowledgments: The authors would like to thank the anonymous reviewers for their valuable comments and suggestions, which helped improve the quality of this manuscript.

Conflicts of Interest: The authors declare no conflicts of interest. The funders had no role in the design of the study; in the collection, analyses, or interpretation of data; in the writing of the manuscript; or in the decision to publish the results.

References

1. Kermack, W.O.; McKendrick, A.G. A contribution to the mathematical theory of epidemics. *Proc. R. Soc. Lond. A* **1927**, *115*, 700–721. [CrossRef]
2. Newman, M.E.J. Spread of epidemic disease on networks. *Phys. Rev. E* **2002**, *66*, 016128. [CrossRef] [PubMed]
3. Pastor-Satorras, R.; Castellano, C.; Van Mieghem, P.; Vespignani, A. Epidemic processes in complex networks. *Rev. Mod. Phys.* **2015**, *87*, 925–979. [CrossRef]
4. Bansal, S.; Grenfell, B.T.; Meyers, L.A. When individual behaviour matters: Homogeneous and network models in epidemiology. *J. R. Soc. Interface* **2007**, *4*, 879–891. [CrossRef] [PubMed]
5. Kivelä, M.; Arenas, A.; Barthelemy, M.; Gleeson, J.P.; Moreno, Y.; Porter, M.A. Multilayer networks. *J. Complex Netw.* **2014**, *2*, 203–271. [CrossRef]
6. Boccaletti, S.; Bianconi, G.; Criado, R.; del Genio, C.I.; Gómez-Gardeñes, J.; Romance, M.; Sendiña-Nadal, I.; Wang, Z.; Zanin, M. The structure and dynamics of multilayer networks. *Phys. Rep.* **2014**, *544*, 1–122. [CrossRef] [PubMed]
7. Funk, S.; Gilad, E.; Watkins, C.; Jansen, V.A.A. The spread of awareness and its impact on epidemic outbreaks. *Proc. Natl. Acad. Sci. USA* **2009**, *106*, 6872–6877. [CrossRef] [PubMed]
8. Granell, C.; Gómez, S.; Arenas, A. Dynamical interplay between awareness and epidemic spreading in multiplex networks. *Phys. Rev. Lett.* **2013**, *111*, 128701. [CrossRef] [PubMed]
9. Granell, C.; Gómez, S.; Arenas, A. Competing spreading processes on multiplex networks. *Phys. Rev. E* **2014**, *90*, 012808. [CrossRef] [PubMed]
10. Wu, Q.; Fu, X.; Small, M.; Xu, X.J. The impact of awareness on epidemic spreading in networks. *Chaos* **2012**, *22*, 013101. [CrossRef] [PubMed]
11. Zhang, H.F.; Xie, J.R.; Tang, M.; Lai, Y.C. Suppression of epidemic spreading in complex networks by local information based behavioral responses. *Chaos* **2014**, *24*, 043106. [CrossRef] [PubMed]
12. Zhang, Y.; Lu, X.; Cui, N.; Tang, J.; Zhang, X. Coevolving dynamics between epidemic and information spreading considering the dependence between vigilance and awareness prevalence. *Complexity* **2021**, *2021*, 5515549. [CrossRef]
13. Li, X.J.; Li, C.; Li, X. The impact of information dissemination on vaccination in multiplex networks. *Sci. China Inf. Sci.* **2022**, *65*, 172202. [CrossRef]
14. Chen, J.; Hu, M.; Cao, J. Dynamics of information-awareness-epidemic-activity coevolution in multiplex networks. *Phys. Rev. Res.* **2023**, *5*, 033065. [CrossRef]
15. Xian, J.; Zhang, Z.; Li, Z.; Yang, D. Coupled information–epidemic spreading dynamics with selective mass media. *Entropy* **2023**, *25*, 927. [CrossRef] [PubMed]
16. Yin, Q.; Wang, Z.; Xia, C. Information-epidemic co-evolution propagation under policy intervention in multiplex networks. *Nonlinear Dyn.* **2023**, *111*, 14583–14595. [CrossRef] [PubMed]
17. Xiong, W.; Zhou, C. Epidemic spreading with an awareness-based adaptive mechanism in temporal multiplex networks. *Front. Phys.* **2023**, *11*, 1285480. [CrossRef]
18. Xu, J.; Li, J.; Han, Z.; Zhu, P. Coupled epidemic dynamics with awareness heterogeneity in multiplex networks. *Chaos Solitons Fractals* **2024**, *187*, 115335. [CrossRef]
19. Feng, M.; Liu, L.; Chen, J.; Xia, C. Heterogeneous propagation processes between awareness and epidemic on signed multiplex networks. *Chaos Solitons Fractals* **2024**, *183*, 114858. [CrossRef]
20. Wang, J.; He, H.; Li, P.; Du, Z.; Xu, X. Epidemic spread dynamics in multilayer networks: Probing the impact of information outbreaks and reception games. *Chaos* **2025**, *35*, 033118. [CrossRef] [PubMed]
21. Gao, M.; Zhu, L.; Shen, S. Epidemic propagation dynamic on the higher-order multilayer network. *Chaos Solitons Fractals* **2025**, *200*, 116922. [CrossRef]
22. Mossong, J.; Hens, N.; Jit, M.; Beutels, P.; Auranen, K.; Mikolajczyk, R.; Massari, M.; Salmaso, S.; Scalia Tomba, G.; Wallinga, J.; et al. Social contacts and mixing patterns relevant to the spread of infectious diseases. *PLoS Med.* **2008**, *5*, e74. [CrossRef] [PubMed]
23. Prem, K.; Cook, A.R.; Jit, M. Projecting social contact matrices in 152 countries using contact surveys and demographic data. *PLoS Comput. Biol.* **2017**, *13*, e1005697. [CrossRef] [PubMed]

Disclaimer/Publisher's Note: The statements, opinions and data contained in all publications are solely those of the individual author(s) and contributor(s) and not of MDPI and/or the editor(s). MDPI and/or the editor(s) disclaim responsibility for any injury to people or property resulting from any ideas, methods, instructions or products referred to in the content.